The Thesis Committee for Dagoberto Garza
Certifies that this is the approved version of the following Thesis:

The Use of High-Strength Reinforcement in Bridge Decks

APPROVED BY
SUPERVISING COMMITTEE:

Oguzhan Bayrak, Supervisor

Anca Ferche, Reader

The Use of High-Strength Reinforcement in Bridge Decks

by

Dagoberto Garza

Thesis

Presented to the Faculty of the Graduate School of

The University of Texas at Austin

in Partial Fulfillment

of the Requirements

for the Degree of

Master of Science in Engineering

The University of Texas at Austin

December 2023

Dedication

...to my parents

Acknowledgements

There have been many people who have impacted my two-year journey at FSEL. This section summarizes my many thanks to those who contributed to this project.

First, I would like to sincerely thank my supervisor, Dr. Oguzhan Bayrak, for the guidance and support provided to me throughout this project. Thanks to Yongjae Yu and Dr. Elias Saqan for their numerous contributions towards the success of this research. I would also like to thank Dr. Anca Ferche for being the reader of my thesis, this thesis greatly benefited from your feedback. This project would not have been possible without funding from the Texas Department of Transportation. The opportunity to work on this project was an invaluable experience, I am very thankful to have contributed towards research on Texas bridges. Additionally, I would like to thank Valley Prestressed Products Inc. for their generous donations of precast, prestressed concrete panels for this project. Special thanks to those I met in the field for their hard work in fabricating the panels.

Many thanks go to Dustin Miller, Hunter Cohen, and Dennis Fillip for their technical expertise during the fabrication of the test specimens. Without your willingness to help in the hot summer and cold winters, the completion of this project would not have been possible. To everyone who helped me during casts and tests, thank you for always lending a hand.

To my parents, Dagoberto and Rosita Garza, your work ethic and morals have inspired me to be who I am today. Thank you for always being there for me. To Diego and Angie, I will forever be thankful for your support. Keep making our parents proud.

Lastly, to Andrea, thank you for your support and encouragement throughout these last two years. In the face of challenges, your resilience and optimism remind me that we can conquer anything together.

Abstract

The Use of High-Strength Reinforcement in Bridge Decks

Dagoberto Garza, MSE

The University of Texas at Austin, 2023

Supervisor: Oguzhan Bayrak

This thesis investigates the performance of high-strength reinforcement in cast-in-place (CIP) bridge decks with precast, prestressed concrete panels (PCPs) as stay-in-place formwork. A total of six deck strip specimens that simulate transverse and longitudinal section details in CIP-PCP bridge decks were constructed and tested to failure under four-point bending. The test variables include reinforcement grade and spacing of reinforcement in the CIP layer. The experimental tests revealed that high-strength reinforcement had a similar crack-control performance as the conventional reinforcement at the same spacing. Increasing the spacing of reinforcement was found to have negative effects on crack-control performance. All specimens with high-strength reinforcement showed increased flexural capacity compared to the specimens with conventional reinforcement. The findings from this experimental program served as the foundation for formulating recommendations regarding the utilization of high-strength reinforcement in CIP-PCP bridge decks.

Table of Contents

List of Tables

List of Figures

Chapter 1: Introduction

1.1. BACKGROUND

Texas Department of Transportation (TxDOT) has extensively employed precast, prestressed concrete panels (PCP) as partial-depth stay-in-place forms in bridge decks since 1963 (Merrill, 2002). The popularity of PCPs in bridge decks is primarily based on the ease of construction, increased safety, and cost savings. Some disadvantages of CIP-PCP bridge decks include cracks in the longitudinal and transverse directions caused by restrained shrinkage (Folliard, 2003).

To highlight key components in CIP-PCP bridge decks, the terminology used in this thesis is illustrated in Figure 1.1-1. The construction procedure comprises of placement of panels on girder flanges, the addition of top mat reinforcement, followed by the placement of cast-in-place (CIP) concrete slab. When PCPs are used as stay-in-place forms in bridge decks, TxDOT specifies a 4" thickness for PCPs with a 4.5" CIP layer, resulting in a total depth of 8.5". The current TxDOT bridge design standards specify #4 reinforcing bars placed at 9 in. for the transverse and longitudinal reinforcement in the top mat.

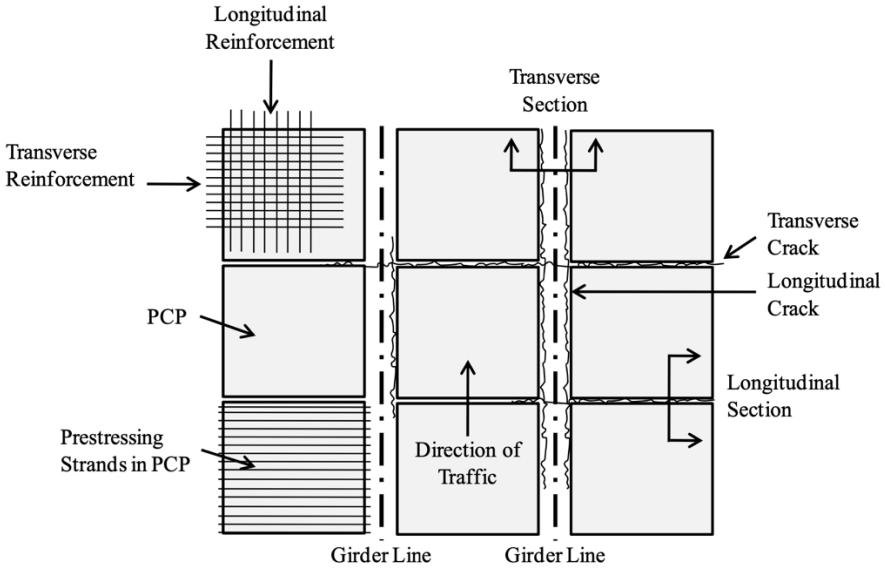

Figure 1.1-1: CIP-PCP Bridge Deck Terminology (Foster, 2010)

Currently, TxDOT does not have guidelines on the use of high-strength reinforcement in CIP-PCP bridge decks. Comparing the conventional reinforcement employed in CIP-PCP bridge decks with high-strength reinforcement, several notable differences emerge that could offer advantages to bridge designers. High-strength reinforcement exhibits larger yield strengths than conventional Grade 60 reinforcement, with yield strengths ranging from 80 to 120 ksi. The high yield strength properties of high-strength reinforcement could result in a reduction in the amount of reinforcement required in Texas bridge decks. In addition, high-strength reinforcement has been found to be more corrosion-resistant when compared to conventional reinforcement (Aldabagh & Alam, 2020). The improved corrosion resistant properties of high-strength reinforcement could lead to increased service life when compared to other reinforcement alternatives (Kahl, 2007).

1.2. RESEARCH SCOPE AND OBJECTIVES

This thesis is part of a larger project to investigate the implementation of high-strength reinforcement in bridges funded by the Texas Department of Transportation. More specifically, the goal of this thesis is to investigate the usage of high-strength reinforcement in CIP-PCP bridge decks.

The experimental program involved the fabrication and testing of six CIP-PCP deck strips that examined the influence of two key variables: rebar grade and rebar spacing. The specimens simulate the transverse and longitudinal sections in CIP-PCP bridge decks. The deck strips were tested in four-point bending. Load capacity and crack-control performance were compared to identify the influence of high-strength reinforcement on CIP-PCP bridge decks. Ultimately, recommendations on the use of high-strength reinforcement were provided based on the experimental results and discussion.

1.3. STRUCTURE OF THESIS

This thesis is divided into six chapters. Chapter 2 focuses on previous studies related to the background of the CIP-PCP bridge deck system and the utilization of high-strength reinforcement in conventional CIP bridge decks. Chapter 3 discusses the experimental program approach used to investigate the use of high-strength reinforcement in bridge decks. Chapters 4 and 5 present and discuss the results from the experimental program and valuable comparisons are made. Chapter 6 presents a summary of the experimental program, findings, and recommendations for additional research.

Chapter 2: Literature Review

When investigating alternatives for bridge deck reinforcement, research on high-strength reinforcement in bridge decks is prominent. Although high-strength reinforcement in bridge decks has been studied, there is limited knowledge on the use of high-strength reinforcement as the top mat reinforcement in CIP-PCP bridge decks. While this thesis focuses on examining the use of high-strength reinforcement in CIP-PCP bridge decks, the following literature review highlights research in the CIP-PCP bridge deck system and high-strength reinforcement in bridge decks. The literature review is not meant to be exhaustive, but rather it is intended to provide context to the work presented in this thesis.

2.1. CIP-PCP Bridge Deck Overview

2.1.1. Buth et al. (1972)

This was one of the first experimental programs investigating the use of precast, prestressed concrete panels (PCPs) in Texas. More specifically, the goal of the study was to investigate the composite action of the PCP and CIP layer working as a unit. The program consisted of a full-scale bridge and slab strips subjected to cyclic and static loads. It was found that the performance of the CIP-PCP bridge deck was acceptable under the loading conditions and that the bond between the CIP and PCP layers was adequate, therefore composite action was achieved.

2.1.2. Merrill (2002)

This paper shares insights on the use of PCPs in bridge deck construction in Texas. According to Merrill (2002), more bridge decks in Texas utilize PCPs as stay-in-place forms when compared to plywood forming and stay-in-place metal forms. The popularity of PCPs in bridge decks is attributed to their positive impact on safety, speed of construction, and cost savings. An

increase in safety is noted when considering the lack of temporary formwork removal. Due to the prestressed feature of PCPs, the speed of construction is increased as there is only a single mat of reinforcement required to be placed, compared to two in cast-in-place (CIP) bridge decks. In addition, the PCPs acting as partial-depth stay-in-place forms decrease the amount of CIP concrete needed to be placed in the field.

2.1.3. Folliard (2003)

To examine the influence of top-mat reinforcement in CIP-PCP bridge decks, it is critical to understand the cracking behavior of this system. This study includes field inspections for two CIP-PCP bridge decks in Texas. The field inspections focused on investigating longitudinal and transverse cracks in the CIP layer. During the inspections, it was observed that the cracks usually occurred at panel edges as shown in Figure 2.1-1. After observing the crack patterns having a close relationship to the location of panels, the influence of the panels in cracking was highlighted. It was found that the rates of shrinkage of the PCP and CIP layers were different, therefore causing a difference in volumetric change of the CIP and PCP layers. This resulted in restrained shrinkage cracking, which was found to be the main reason for cracking in CIP-PCP bridge decks.

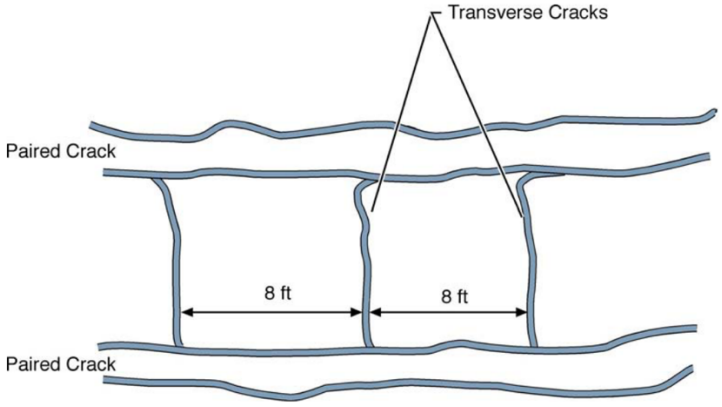

Figure 2.1-1: Typical cracking pattern in CIP-PCP Bridge Decks (Folliard, 2003)

2.1.4. Kwon (2012)

This experimental program focuses on design recommendations to lower the cost of CIP-PCP bridge decks. Part of this study examines the behavior of transverse reinforcement alternatives in the CIP layer. To compare the standard transverse reinforcement at the time (#5 at 6 in.), a CIP-PCP bridge deck incorporating standard reinforcement details and transverse reinforcement alternatives was constructed. The reinforcement alternatives included welded-wire reinforcement (D20 at 6 in.) and a reduction in reinforcement from #5 at 6 in. to #4 at 6 in.

Based on monitoring the bridge deck for 75 days after casting, limited data was collected to compare the behavior of the bridge decks with differing reinforcement arrangements. Ultimately it was found that the transverse reinforcement alternatives did not result in considerable differences in bridge deck behavior when compared to the standard reinforcement details.

2.2. HIGH-STRENGTH REINFORCEMENT IN BRIDGE DECKS

2.2.1. Frosch et al. (2014)

This experimental program focused on the influence of different types of reinforcement and reinforcement spacing in bridge decks. Slab specimens were used to examine the crack behavior of the different arrangements of reinforcement. The dimensions of the slab specimens were specified as 3 feet wide, 16 feet long, and 8 in. deep.

A total of seven reinforcement types were examined in this study, including high-strength reinforcement (MMFX II). To evaluate the influence of bar spacing of high-strength reinforcement, slab specimens with 6-, 12-, and 18-inch rebar spacing were examined for crack-control performance. As shown in Figure 2.2-1, the method of testing the slab specimens was a constant moment test.

This study revealed that as the reinforcement spacing increases, crack widths increase, and the number of cracks decreases. Additionally, it was found that high-strength reinforcement exhibited crack-control performance similar to conventional reinforcement at the same spacing

before yielding. Ultimately, it was found that the Frosch (1999) crack width model could be applied to concrete members with high-strength reinforcement up to a bar stress of 80 ksi.

Figure 2.2-1: Constant moment test for slab specimens by Frosch et al. (2014)

2.2.2. R. S. Kareem et al. (2020)

The program focused on comparing the influence of high-strength and conventional reinforcement on the load capacity and crack-control performance of bridge decks. Slab segments were tested in four-point bending, as shown in Figure 2.2-2. The slab segments were 35.4 in. wide, 165.4 in. long, and 7.8 in. deep. Additionally, the specimens consisted of two mats of reinforcement.

For this study, service levels were determined when reinforcement stress reached 60% of yield stress. It was found that a 1:1 replacement of conventional reinforcement with high-strength reinforcement resulted in an increase of flexural capacity. At the same spacing, smaller crack widths were observed at service levels for the specimens containing high-strength reinforcement, compared to those with conventional reinforcement. Additionally, it was found that specimens with high-strength reinforcement at a reduction of 40% reinforcement area resulted in a similar crack width as the control specimens at service limits. Ultimately, it was found that at service loads, a reduction of reinforcement did not negatively impact crack-control performance or flexural capacity.

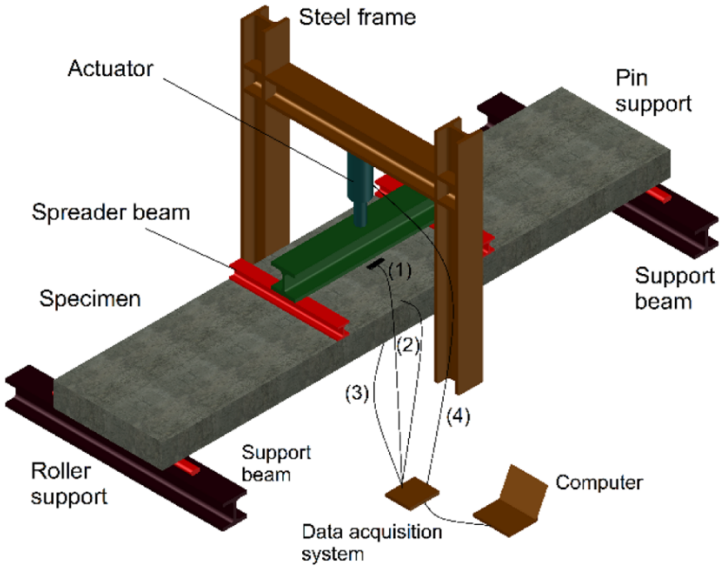

Figure 2.2-2: Four-point bending test setup used by R. S. Kareem et al. (2020)

Chapter 3: Experimental Program

This chapter describes the experimental program used to investigate the use of high-strength reinforcement in CIP-PCP deck strip specimens. This includes specimen design, fabrication, test setup and instrumentation, and testing procedures.

3.1. Specimen Design and Test Matrix

To efficiently observe and compare the use of high-strength reinforcement in CIP-PCP bridge decks, this study utilized deck strip specimens, similar to those tested by Frosch et al. (2014) and R. Kareem (2020). These specimens simulate the reinforcement details of transverse and longitudinal reinforcement at the joints of precast panels, which is where cracks are likely to occur in CIP-PCP bridge decks. The deck strip specimens consist of two layers: the PCP and CIP. The PCPs used for this study measured at 8'-0"x8'-0"x0'-4". The PCP layer mimicked the placement of panels on a girder line or along the girder. Each test specimen had two PCPs in the PCP layer. The panels were separated 7" in the transverse direction to allow for placement of shear connectors, similar to construction practice. Ideally, in the longitudinal direction, the side of one panel would be perfectly flush to the neighboring panel. To accommodate for slight imperfections in the PCPs side face, the panels were provided with a 1-½" separation to allow for concrete placement between the panels, in order to simulate an ideal panel butt next to one another. The CIP layer simulated the reinforced cast-in-place concrete layer in a CIP-PCP bridge deck. This layer had reinforcement in the longitudinal and transverse directions. The arrangement of panels and reinforcement with transparent girder lines are shown in Figure 3.1-1.

A total of six deck strip specimens with varying reinforcement grades and spacing were studied. Three specimens focused on testing the longitudinal reinforcement and three focused on

the transverse reinforcement. Each set of specimens had three distinct reinforcement arrangements: 1) Grade 60 #4 at 9 in., 2) Grade #4 100 at 9 in., and Grade 100 #4 at 15 in. Specimens with reinforcement at 9 in. and 15 in. had a total bar area of 2 in.^{2} and 1.2 in.^{2}, respectively. The specimens reinforced with Grade 60 #4 bars at 9 in. were used as the control specimens, since it represents the current TxDOT reinforcement standard for CIP-PCP bridge decks. The specimens with Grade 100 #4 at 9 in were used to investigate how high-strength reinforcement with the same spacing as the control specimen spacing influences load capacity and crack-control performance. The specimens with Grade 100 #4 at 15 in. examined the use of a reinforcement yield strength-to-reinforcement area product similar to the control specimen, which would result in similar load capacities between the specimens.

The reinforcement arrangement is shown in Table 3.1-1 with the reinforcement bolded indicating the focus of the test. The longitudinal specimens examined the longitudinal reinforcement, which is denoted with an "L" as the first letter of the specimen ID. Similarly, the transverse specimens are denoted with a "T" as the first letter of the specimen ID, which examines the transverse reinforcement. For the longitudinal specimens, the reinforcement provided in the transverse direction was similar to the current TxDOT requirements, Grade 60 at 9 in.. These same details were kept for the longitudinal reinforcement for transverse specimens. The primary layer of reinforcement being examined is shown in Figure 3.1-1. This figure also shows the conventional reinforcement arrangement in the opposite direction.

Table 3.1-1: Test Matrix

Specimen ID	Top-mat Longitudinal Reinforcement	Top-mat Transverse Reinforcement
TN	Grade 60 at 9 in.	**Grade 60 at 9 in.**
TH1	Grade 60 at 9 in.	**Grade 100 at 9 in.**
TH2	Grade 60 at 9 in.	**Grade 100 at 15 in.**
LN	**Grade 60 at 9 in.**	Grade 60 at 9 in.
LH1	**Grade 100 at 9 in.**	Grade 60 at 9 in.
LH2	**Grade 100 at 15 in.**	Grade 60 at 9 in.

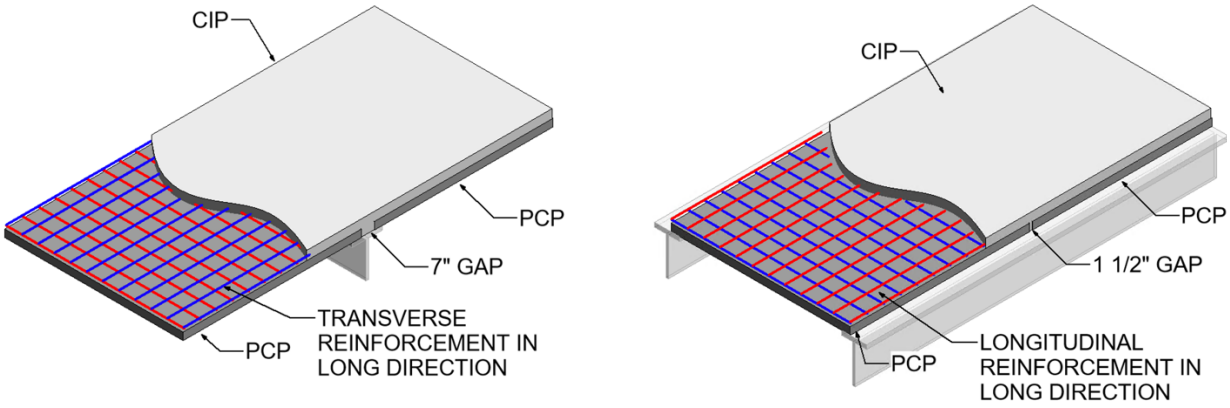

a) Transverse Deck Strip Specimen

b) Longitudinal Deck Strip Specimen

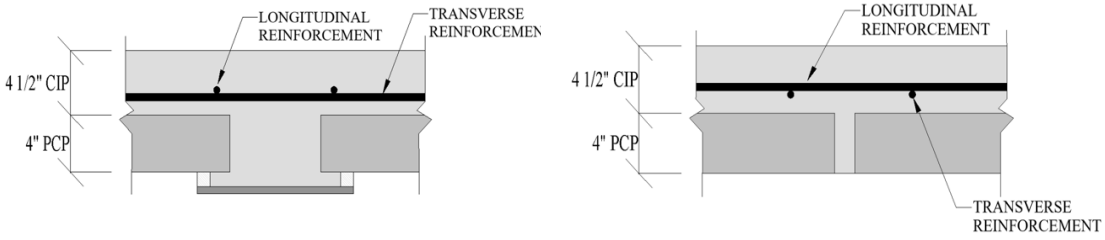

c) Transverse Panel Joint

d) Longitudinal Panel Joint

Figure 3.1-1: Deck strip specimen details

3.2. SPECIMEN FABRICATION

3.2.1. Precast Prestressed Concrete Panels

Twelve precast, prestressed concrete panels were supplied by Valley Prestressed Products Inc. The concrete panels were constructed following TxDOT standard PCP details(*Prestressed Concrete Panel Fabrication Details*, 2023). Transverse reinforcement consisted of prestressed strands spaced at 6 in. with a tension force of 14.4 kips per strand. Longitudinal reinforcement consisted of #3 rebar spaced at 6 in. During the fabrication, the panels were broom-finished to assist in composite action with the CIP layer of concrete. The PCP reinforcement and finished PCPs are shown in Figure 3.2-1.

a) PCP Reinforcement

b) Finished PCPs

Figure 3.2-1: PCP fabrication

3.2.2. Deck Strip Specimens

For each specimen, 120-ohm strain gauges with a gauge length of 5 mm were applied to the reinforcement at critical locations. To ensure proper installation of a strain gauge, approximately one inch of the reinforcement surface was ground using a pneumatic angle grinder to smooth the bar surface. After the reinforcement surface was smoothed and cleaned with acetone,

the application of strain gauge was achieved using CN adhesive, as shown in Figure 3.2-2. Afterward, the strain gauges were coated with M-Coat A for moisture resistance. Finally, each strain gauge was further protected with SB tape, Scotch VM tape, and an application of epoxy.

Figure 3.2-2: Typical strain gauge application

The rebar near the center of the specimen had strain gauges spaced at 9 in. while all other strain gauges were spaced at 18 in. The location of strain gauges for specimens with reinforcement with 9 in. spacing and 15 in. spacing are shown in Figure 3.2-3.

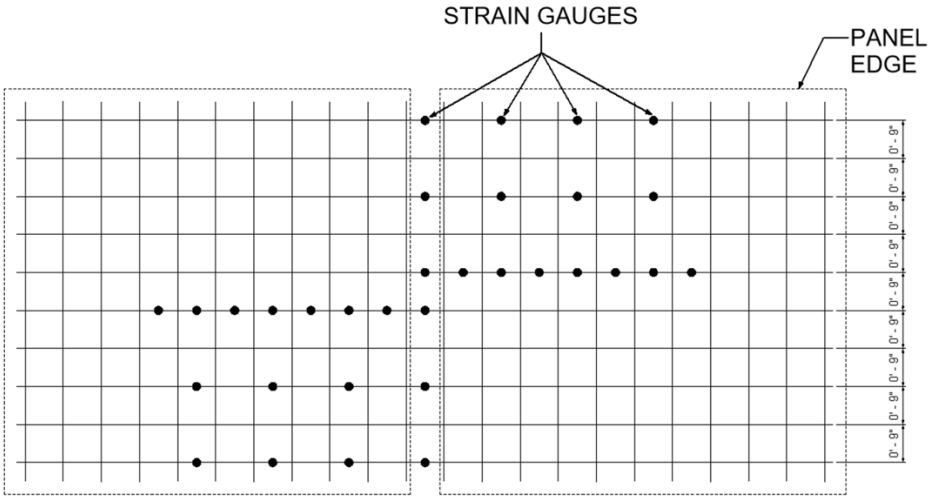

a) Strain gauge location for specimens with reinforcement spaced at 9 in.

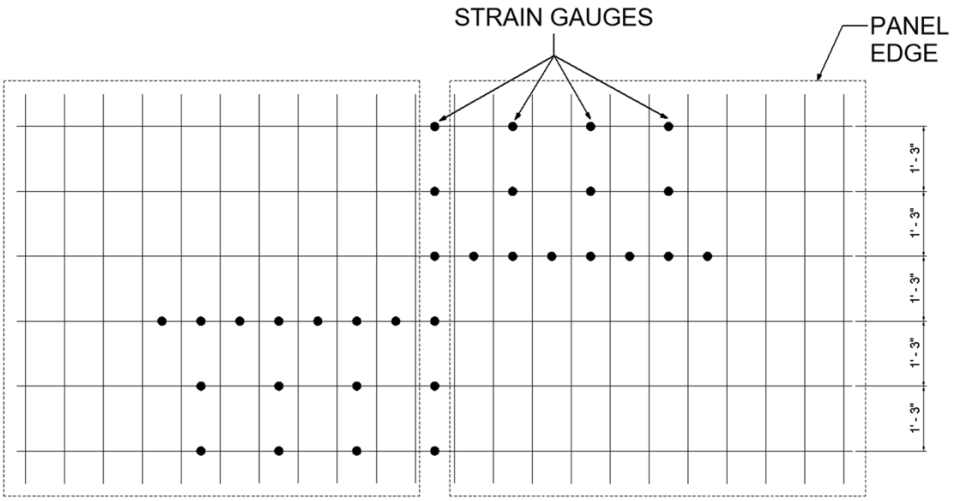

b) Strain gauge location for specimens with reinforcement spaced at 15 in.

Figure 3.2-3: Strain gauge locations

After strain gauges were attached to the reinforcement, the strain gauge wires were labeled to accurately connect them to the data acquisition system (DAQ). Once rebar was placed on the specimen, they were routed through and protected using plastic bags, which is shown in Figure 3.2-4.

Figure 3.2-4: Typical strain gauge arrangement and protection

Two different processes were used to simulate the panel joints in the longitudinal and transverse directions. These processes are provided in the next few sections:

3.2.2.1. Transverse Specimens

The transverse deck strip specimens simulate the transverse reinforcement details in CIP-PCP bridge decks. To mimic a girder line in the transverse direction, a simulated girder line was used. The simulated girder line consisted of a 12"x96"x1/2" steel plate with 7/8" diameter shear studs spaced at 12" O.C. The purpose of the shear studs was purely to replicate girder line details and were not intended to add any capacity to the specimen. The girder line was then carefully placed on the soffit. Bedding strips were then glued to the simulated girder line, which is where the panels were placed. For each transverse specimen, the panels were roughly 7" apart to accommodate the shear studs from the simulated girder line. These details are shown in Figure 3.2-5.

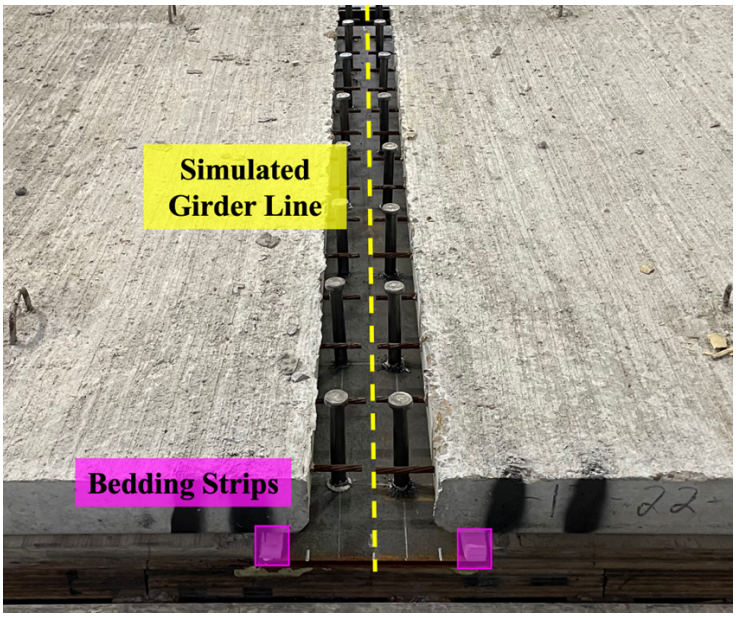

Figure 3.2-5: Transverse specimen panel joint details

3.2.2.2. Longitudinal Specimens

The longitudinal deck strip specimens simulate the longitudinal reinforcement details in the CIP-PCP bridge decks. The PCPs were placed with a 1 ½-in. gap which was filled with the same concrete used for the CIP of the specimen, as shown in Figure 3.2-6. The concrete between the joints allowed for an idealized panel-to-panel interaction in a at simulated longitudinal panel joint.

Figure 3.2-6: Longitudinal specimen panel joint details

Once the panels were in place, the corresponding transverse and longitudinal reinforcement were then located on 1-in. chairs to accommodate for adequate cover. In addition, Meadow Burke anchors were tied to the reinforcement to easily move the specimen from the casting area to the testing setup via an overhead crane.

It is important to note that before concrete placement, the face of the panels was sprayed with water to achieve a saturated surface dry condition, as shown in Figure 3.2-7. For each CIP layer placement, concrete vibrators were used to ensure proper concrete consolidation. When casting each deck strip specimen, concrete was first placed at the panel joint to ensure the placement of concrete at the panel joint. This was followed by concrete placement of the entire CIP layer. To easily attach instrumentation on the CIP surface, the top layer was screeded at the end of the concrete placement.

a) Concrete Placement of Longitudinal Panel Joint

b) Concrete Placement of Transverse Panel Joint

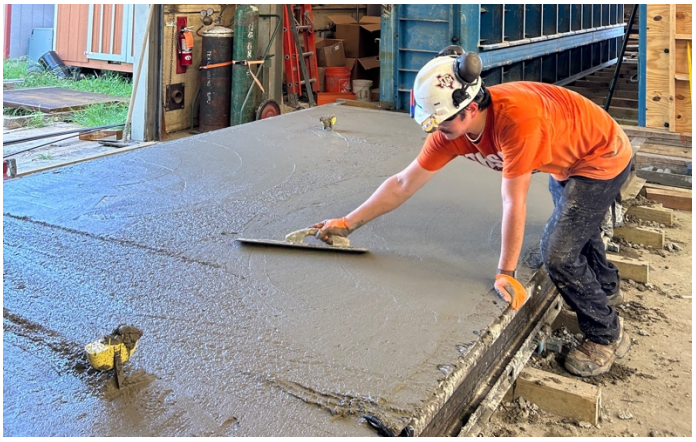

c) CIP Layer Placed and Finishing

Figure 3.2-7: Concrete placement procedures

Although not all specimens utilized the same concrete batch for the CIP layer, the same concrete mix design was ordered for each specimen. The concrete mix prescribed was specified to have a minimum 28-day compressive strength of 4000 psi. The concrete mix design was as summarized in Table 3.2-1. Before placement of the CIP layer, the slump was measured following ASTM C143.

Table 3.2-1: Concrete mixture design

Material Type	Description	Weight
Cement	ASTM C-150 Type I/II	452 lb/cy
Fly Ash	Class F	112 lb/cy
Coarse Aggregate	1" Concrete Rock	1905 lb/cy
Fine Aggregate	Concrete Sand	1363 lb/cy
Water	Water	30 gal/cy
Admixture	ASTM C494 type A/F (SikaPlast -330 GP)	--
Admixture	ASTM C494 type B/D (SikaTard 440)	--

Once the CIP layer was placed, the specimen was covered with plastic sheeting to allow for curing. Each transverse deck strip specimen measured at a final length of 16'-7", width of 8'-0", and height of 0'-8 ½". Each longitudinal deck strip specimen measured at a final length of 16'-1 1/2", width of 8'-0", and height of 0'-8 ½". After specimens were de-molded and reached a compressive strength of 4000 psi, they were moved to the testing frame.

3.3. MATERIAL TESTS

3.3.1. Concrete materials

For each specimen's CIP layer placement, (25) 4 in. x 8 in. concrete cylinder samples were collected, as shown in Figure 3.3-1. Additionally, concrete cylinder samples were collected for PCP material property testing. The cylinders were demolded at 24 hours after cast and submerged in a water tank at ambient temperature. These concrete samples were used to record the 28-day and test-day compressive strength following ASTM C39. The concrete cylinders were also utilized to record split tensile strength and modulus of elasticity on test day following ASTM 496 and ASTM 469. The results for the concrete material tests are presented in Table 3.3-1.

a) Concrete cylinders from CIP placement

b) Concrete cylinders prepared at precast fabricator

Figure 3.3-1: Preparation of concrete cylinders

Table 3.3-1: PCP and CIP concrete material test results

Specimen ID	Type	f_c' (psi)	f_t (psi)	E_c (psi)
TN	CIP	6516	436	4553
	PCP	9784	456	6321
TH1	CIP	4898	442	5019
	PCP	9347	488	6505
TH2	CIP	5539	628	5304
	PCP	8782	615	6572
LN	CIP	6098	617	5919
	PCP	8323	748	6779
LH1	CIP	6795	429	5315
	PCP	9409	490	6103
LH2	CIP	5440	453	5980
	PCP	9193	600	7360

3.3.2. Reinforcement materials

To examine the material properties of the reinforcement used in this study, longitudinal tension tests following ASTM A370 were performed. For high-strength reinforcement, the yield

strength was determined using the 0.2% offset method as specified in ASTM A370. The yield and ultimate stress results for flexural reinforcement in each specimen are shown in Table 3.3-2. The complete stress-strain results for the tension tests are shown in Appendix A: Stress-Strain Curves of Steel Reinforcement Material Tests.

Table 3.3-2: Steel reinforcement material test results

Specimen	Reinforcement Type	Grade	f_y (ksi)	f_u (ksi)
TN	ASTM A615	60	63.9	104.3
LN			73.8	114.3
TH1	ASTM A1035	100	136.9	172
TH2				
LH1				
LH2				

3.4. TEST SETUP, INSTRUMENTATION, AND TESTING PROCEDURE

3.4.1. Test Setup

To analyze the crack-control characteristics of different reinforcement arrangements in the CIP layer of the deck strip specimens, a four-point bending test setup was used. The testing frame consisted of four hydraulic rams under a loading frame. The resulting load from the hydraulic rams was evenly distributed across the specimen by two 8’-0” long welded rods spaced at 5’-0” at the center of the loading frame.

After placing the specimen on the loading frame, pin and roller supports were placed on each end of the specimen. The pin support consisted of a 2 in. diameter welded rod on a steel plate to restrain lateral translation. Comparatively, the roller support consisted of a 2 in. placed on the steel plate to allow for lateral translation. Underneath each support, a rubber mat was placed to

accommodate for uneven finished CIP surface. After the supports were positioned, the reaction beams were placed on the supports. Each reaction beam had two 100-kip load cells anchored with a rod and reaction nut. Isometric and elevation views of the test setup are shown in Figure 3.4-1 and Figure 3.4-2. It is important to note that before testing, supporting jacks were placed at the corners of the specimen to prevent unwanted deformations and stresses under self-weight prior to testing the specimen, as shown in Figure 3.4-3.

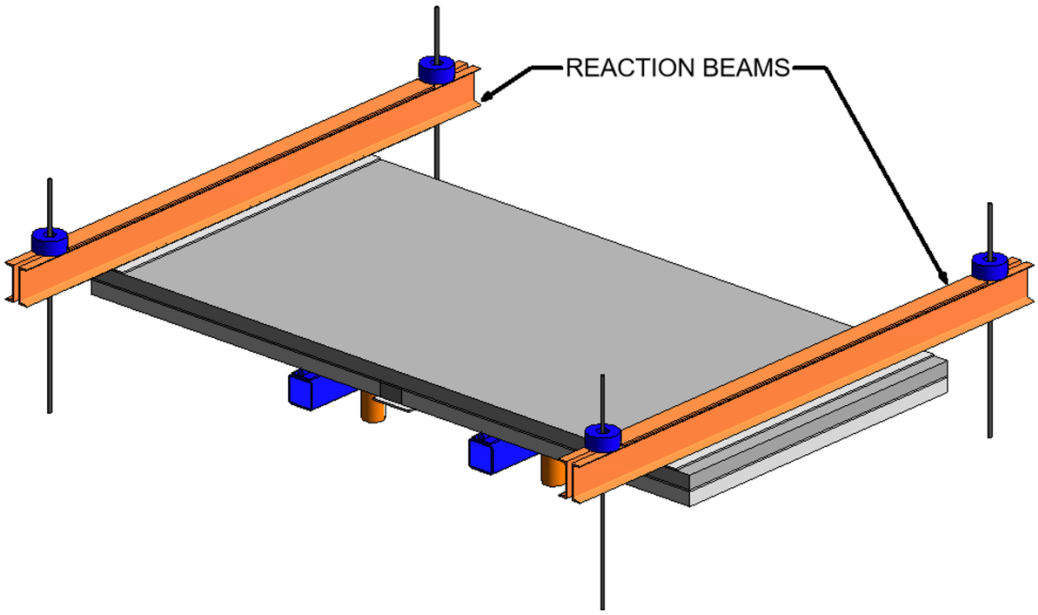

Figure 3.4-1: Test setup (isometric view)

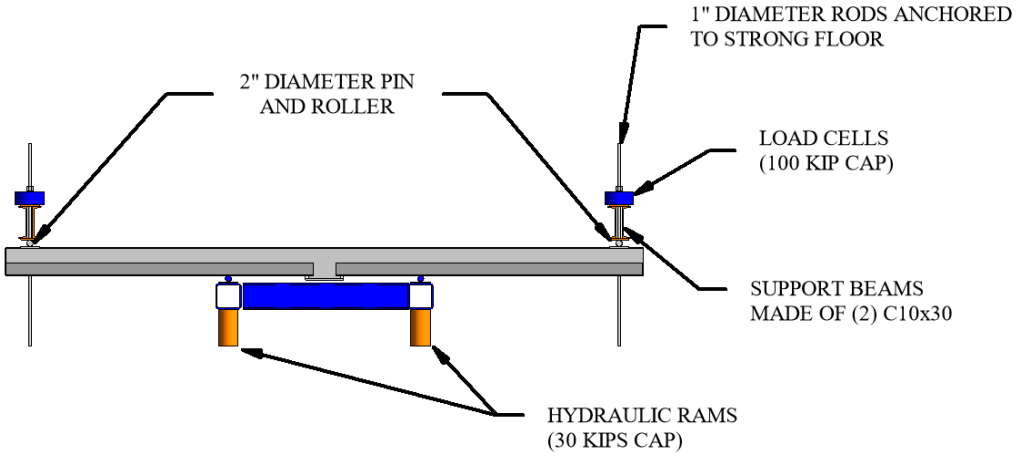

Figure 3.4-2: Test setup (elevation view)

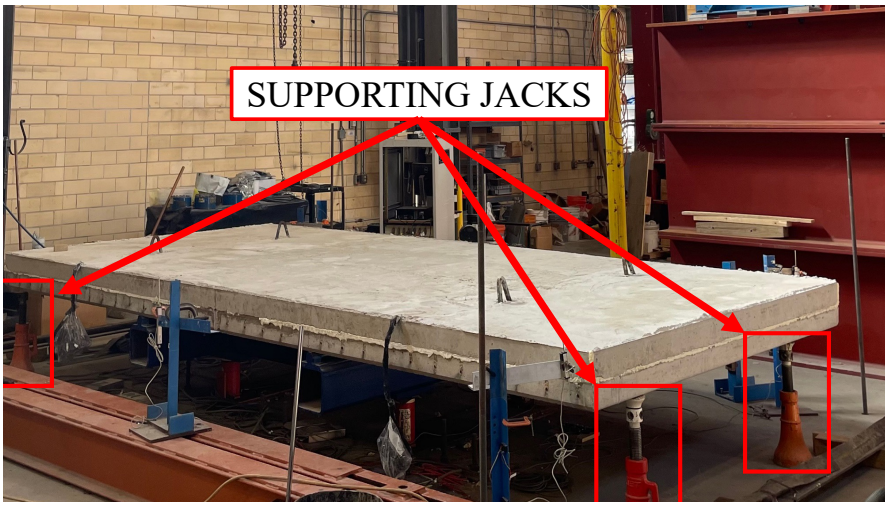

Figure 3.4-3: Placement of supporting jacks prior to testing

3.4.2. Instrumentation

To monitor the specimen behavior during testing, five distinct types of instrumentation were used: load cells, linear potentiometers (L-pots), strain gauges, pi-shape displacement transducers, and Optotrak System.

The strain gauges applied to the reinforcement were used to measure the strain of the reinforcement. The strain would then be used to calculate reinforcement stress using the corresponding material tests. Further discussion on the use of strain gauge readings are presented in Section 4.3.

100-kip capacity load cells were used to measure the reaction forces at each end of the deck strip specimen. A total of six L-pots were used to measure displacement. Two L-pots measured the center displacement on each side of the specimen. Two L-pots measured the displacement of each end for both reaction beams. The goal of L-pot locations was to plot load vs. deflection and to measure rigid body motion during testing. The location of the L-pots on one side of a specimen is shown in Figure 3.4-4.

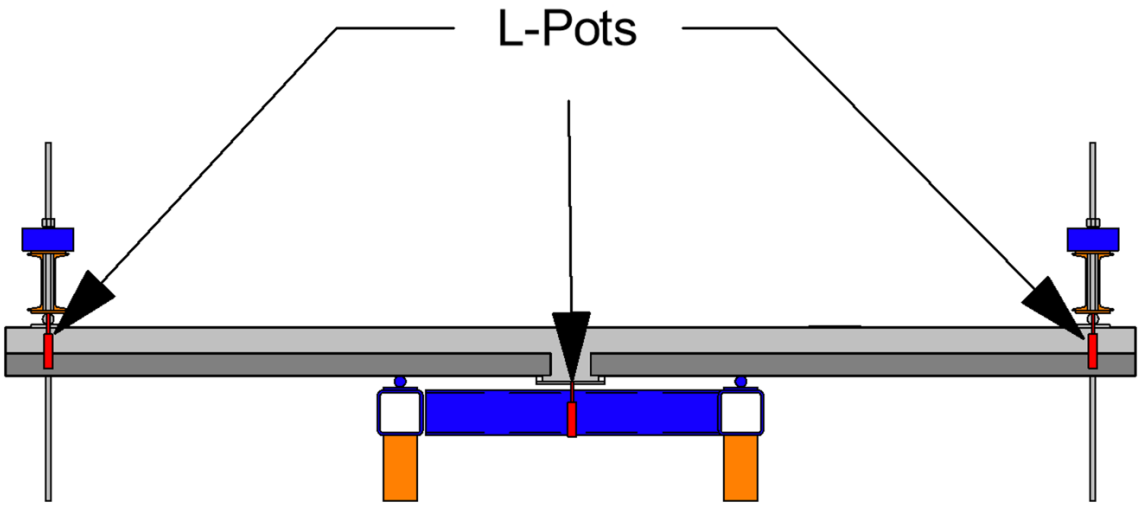

Figure 3.4-4: Test setup L-Pot locations

The Optotrak System was used to measure crack widths throughout the test. The Optotrak System comprises of the Optotrak camera and Optotrak markers. This system recorded the location of the Optotrak markers in 3-dimensional coordinates throughout the test. The markers were placed in an orthogonal grid pattern to cover the center of the specimen. The spacing of the markers was

6” in each direction. To simplify data processing, the use of Optotrak computer software was used to align the markers in the XY plane. For clarity, the orientation of the Optotrak markers is shown in Figure 3.4-5.

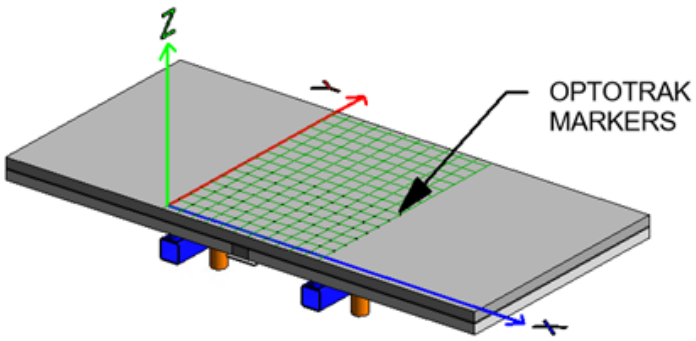

Figure 3.4-5: Orientation of Optotrak markers

In addition, PI-shape displacement transducers (PI-gauge) were installed on the side surface of the specimen to monitor potential separation of PCP and CIP layers. The specimens that had PI-gauges installed were TH2, LN, LH1, and LH2. The locations of the PI-gauges were placed relative to the center of the specimen and a schematic of the installation is shown in Figure 3.4-6.

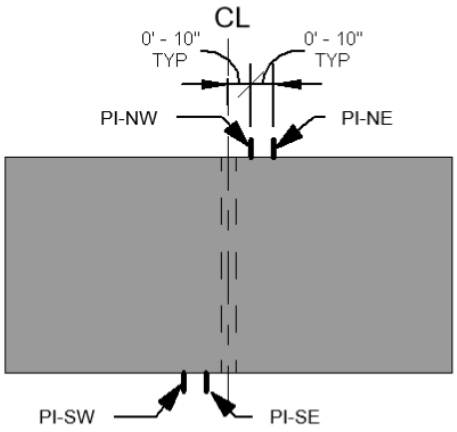

a) Plan view of specimen with PI-gauge locations

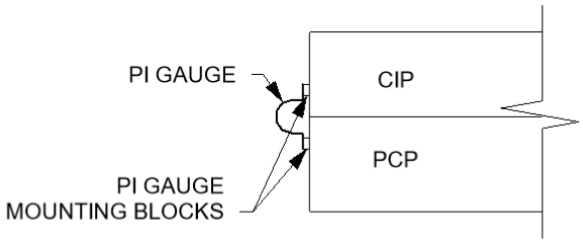

b) Installation of PI-Gauge between CIP and PCP layers

Figure 3.4-6: PI-gauge location and installation

3.4.3. Testing Procedure

Before starting the deck strip four-point bending test, L-pots were placed at the respective locations, and the supporting jacks were removed. The data acquisition system (DAQ) was then zeroed and started recording at load from load cells, displacement from L-pots, and strain from strain gauges. The Optotrak System started recording the Optotrak markers at the same time as the DAQ started recording.

Afterward, each nut anchoring the reaction beams to the strong floor was tightened with a wrench so that 0.5 kips was measured at each load cell, resulting in a total pre-load of 1 kip at each end of the specimen. The load was then applied at 3-kip increments until excessive crack widths occurred. At this stage of testing, cracks were marked and measured using a crack card at each load interval. After crack widths were no longer able to be measured by crack card, the load was increased until failure. Failure was determined when the load measured was no longer increasing or when excessive delamination between the CIP-PCP interface occurred.

Chapter 4: Experimental Results

The experimental results for the deck strip testing are presented and discussed in this chapter. This chapter will highlight the load capacity and crack-control results in the longitudinal and transverse directions. In addition, the data processing methodology for rebar stress will be explained.

4.1. Overview of Deck Strip Test

The applied loads, P, the reaction forces, R, and moment diagram for the four-point bending test are shown in Figure 4.1-1. R1 and R2 are the reactions read from the load cells. P is representative of the force applied by the hydraulic rams. The moment, $M_{Test,}$ is the resulting moment from self-weight and applied load, P.

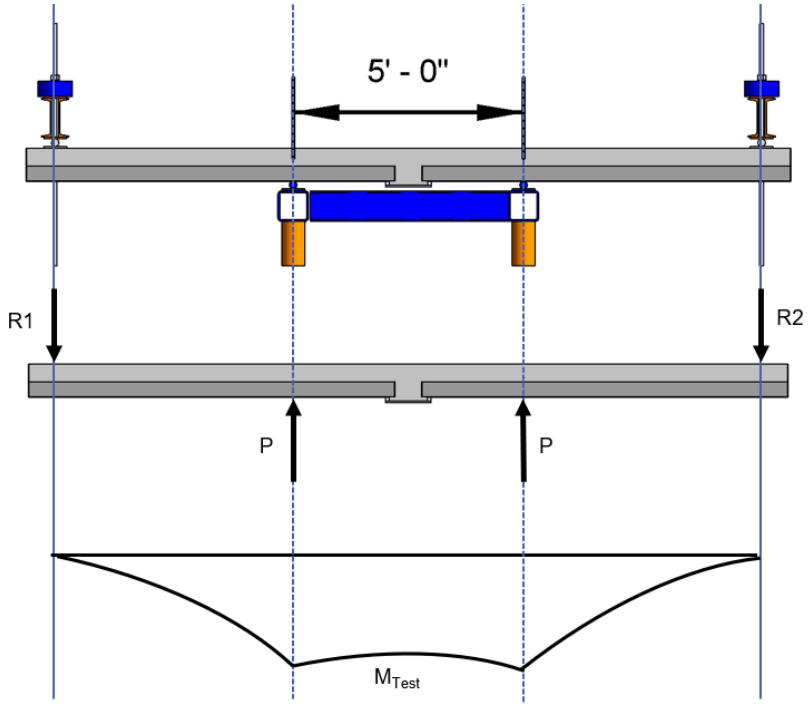

Figure 4.1-1: Resulting forces and uniform moment from four-point bending test

4.2. LOAD CAPACITY

This section presents the load capacity results in the transverse and longitudinal specimens. The ultimate applied load, which is the maximum load read from the load cells, and corresponding deflection at the center of the slab are shown in Table 4.2-1.

Table 4.2-1: Load-Deflection results summary

Specimen ID	Ultimate Applied Load (kips)	Center Deflection (in.)
TN	17.4	0.9
TH1	49.7	6.1
TH2	26.3	5.7
LN	22.3	2.7
LH1	34.6	3.3
LH2	25.5	4.3

4.2.1. Transverse Specimens

The load-deflection curves for each transverse specimen are shown in Figure 4.2-1. All specimens failed in flexure. Specimen TH1 had the largest load capacity out of the three transverse specimens. Additionally, specimen TH2 had a larger load capacity when compared to the control specimen (TN).

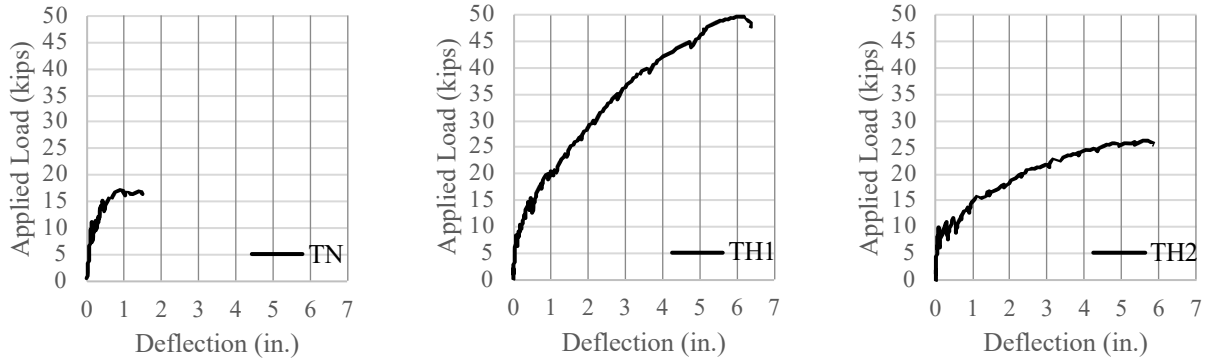

a) TN (Grade 60 @ 9 in.) b) TH1 (Grade 100 @ 9 in.) c) TH2 (Grade 100 @ 15 in.)

Figure 4.2-1:Load-Deflection for transverse specimens

4.2.2. Longitudinal Specimens

The load-deflection curves for each longitudinal specimen are shown in Figure 4.2-1. The LN specimen failed in flexure, while specimens LH1 and LH2 exhibited local failure on one side of the specimens, as shown in the crack patterns in Figure 4.3-5. This is believed to have occurred due to the inability of the CIP-PCP interface to carry the shear forces. This localized failure resulted in the lack of load plateau at the end of the tests. Although this was the case, specimens with high-strength reinforcement had larger load-carrying capacity than the control specimen (LN).

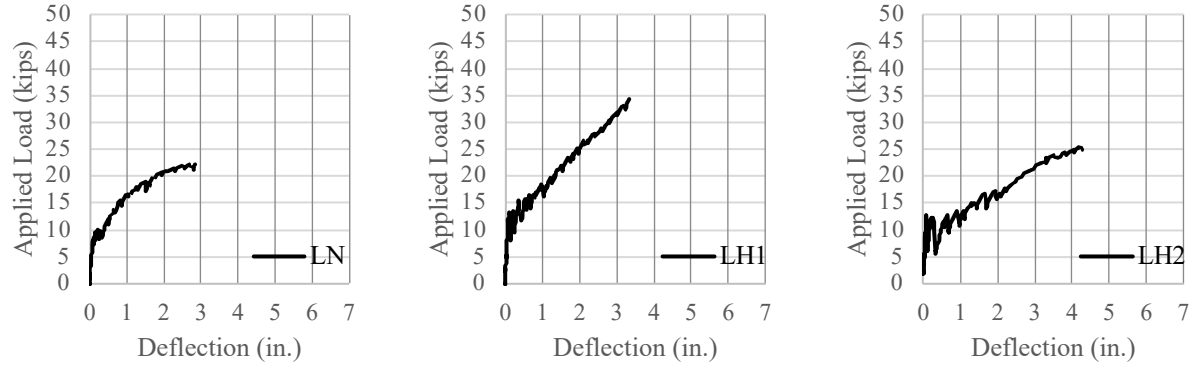

a) TN (Grade 60 @ 9 in.) b) TH1 (Grade 100 @ 9 in.) c) TH2 (Grade 100 @ 15 in.)

Figure 4.2-2: Load-Deflection for longitudinal specimens

4.3. CRACK-CONTROL PERFORMANCE

This section presents the method of evaluating the crack control performance in the transverse and longitudinal directions. In addition, the crack-control performance results are provided and compared in this section.

4.3.1. Load and Crack Width as Indicators for Crack-Control Performance

The reinforcement stress can be determined from the strain value measured by the strain gauges on the top-mat reinforcement with the material test results. Due to the location of the strain gauges and random propagation of cracks, rebar stress at the crack was not efficiently captured

from the strain gauges measurements, as shown in Figure 4.3-1. Consequently, this limitation led to challenges in establishing meaningful comparisons between the rebar stresses obtained from the strain gauges and the crack widths. For this reason, the applied load was used to evaluate the crack-control performance.

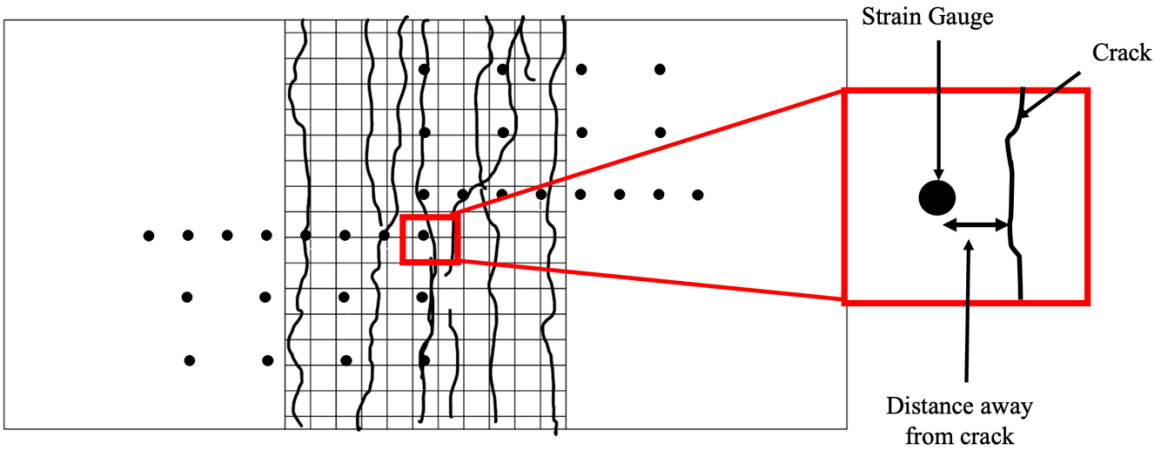

Figure 4.3-1: Strain gauge location limitation

4.3.2. Crack Width Readings

For each test, crack widths were measured following two methods: visual crack card readings and Optotrak measurements. The data from the Optotrak consisted of XYZ coordinates for each marker for the duration of the test. This data was used to track changes in distance from one marker to another.

As the load is being applied to the specimen, deflections cause a change in the angle of the CIP surface. Due to this angle change, crack widths could not be calculated based on only the change in the x direction (as shown in Figure 3.4-5). As shown in Figure 4.3-2, as deflections occur due to applied load, a change in x and z are considered when measuring crack widths. When measuring the distance between the markers, L1 and L2, were calculated using the absolute distance. By this method, if a crack does not occur between the markers, measurements L1 and L2

would be the same length. Comparatively, when there was a difference in length detected, a crack width was calculated and recorded.

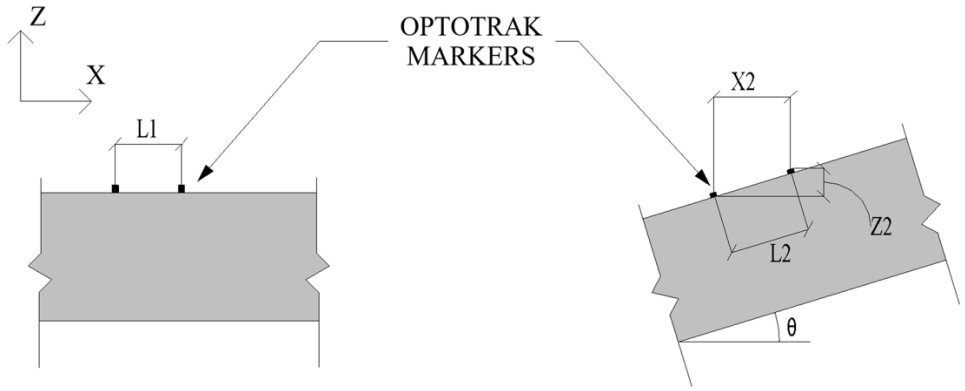

Figure 4.3-2: Optotrak markers data processing methodology

Maximum crack width during the test was collected via visual crack card readings. These visual crack card readings are compared to the maximum crack width measurement obtained using the Optotrak system, as shown in Figure 4.3-3. When comparing the two readings, it is evident that the Optotrak had slightly larger crack width measurements compared to the visual crack card readings. The slight difference in reading could be due to human error in identifying and reading the largest crack width. For this reason, the crack width measurements collected by Optotrak were used for comparisons as it is a more accurate method to collect crack widths and it had the capability to collect measurements throughout the majority of the testing region.

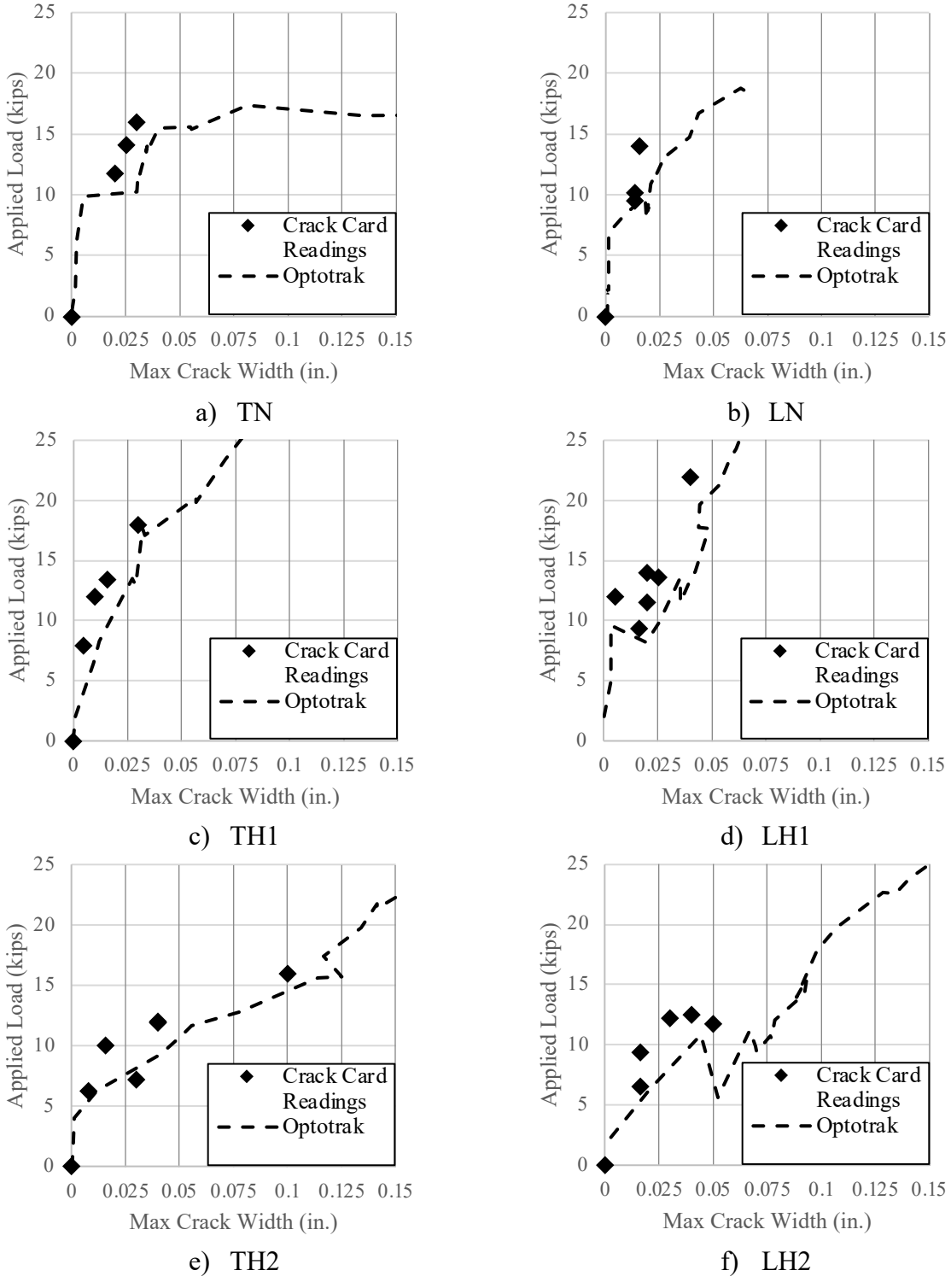

Figure 4.3-3: Optotrak and visual crack card reading comparison

To further validate the Optotrak data, the average surface strains measured by Optotrak were compared to surface strains calculated by nonlinear sectional analysis. The sectional analysis performed utilized the concrete compressive strength from the CIP layer, material properties of reinforcement, and cross-section details including specimen geometry and flexural reinforcement. Aspects not considered in the sectional analysis include CIP-PCP interaction, prestressed strands from PCP, differing concrete compressive strength in PCP and CIP layers, and tension stiffening effects. Figure 4.3-4 illustrates the comparison between the test results obtained from Optotrak and sectional analysis results. In the figure, the test results show the average surface strain measured from the Optotrak plotted against the resulting moment from the applied load and self-weight of the specimen. The resulting surface strain from the test results had similar trends as the idealized sectional analysis.

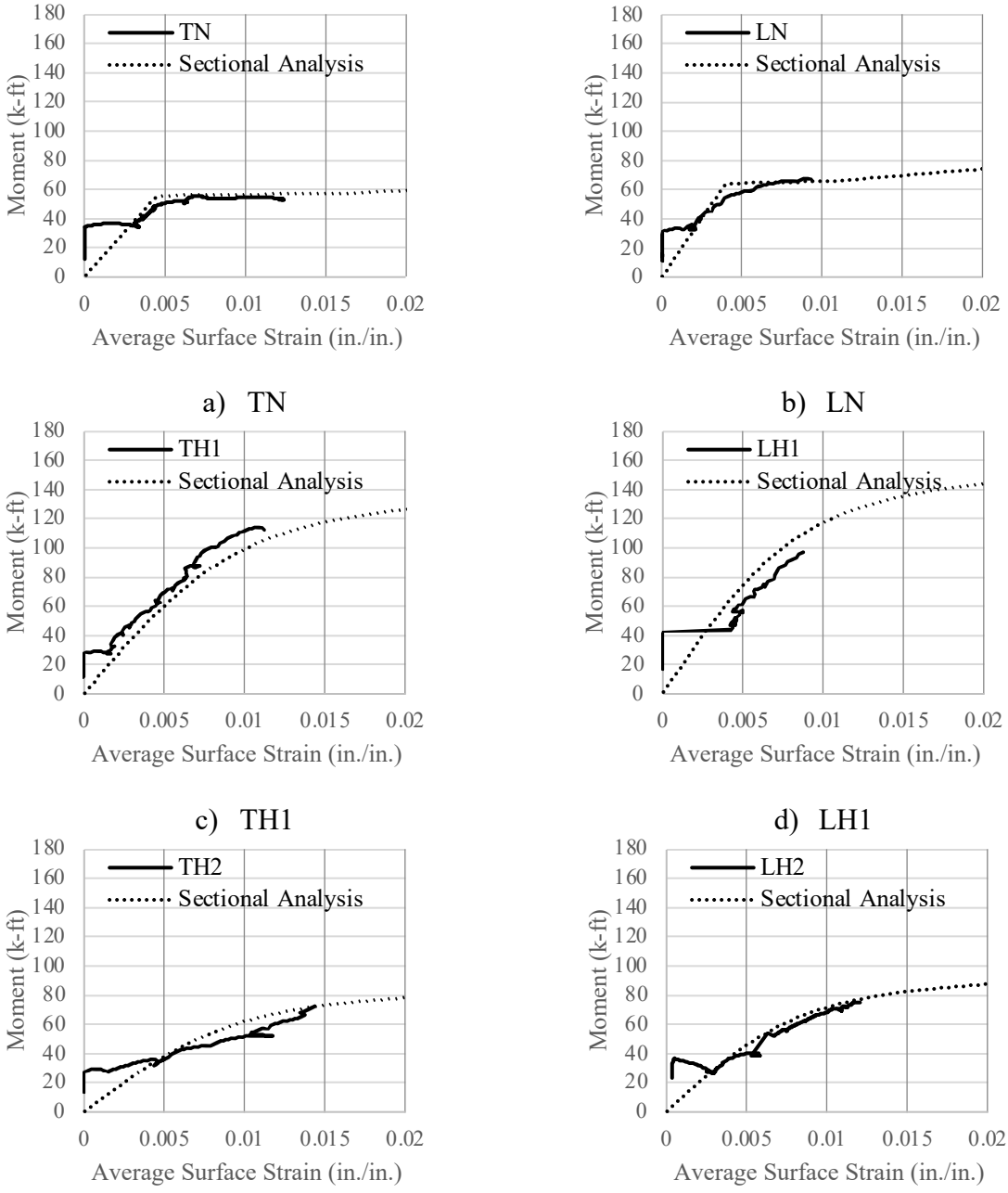

Figure 4.3-4: Simplified sectional analysis and test results comparison

4.3.3. Crack-control Observations

When first crack was detected a drop in load was measured. The moment resulting from the applied load prior to cracking was used to calculate the modulus of rupture for each specimen. As shown in Table 4.3-1, cracking occurred between $4.7\sqrt{f_c'}$ and $6.3\sqrt{f_c'}$, with f'_c being the compressive strength of concrete of the CIP layer on the day of test.

Table 4.3-1: Concrete tensile stresses for initial crack

	M_{cr}(k-ft)	f_r (psi)	f_c' (psi)	$f_r/\sqrt{f_c'}$
TN	39.9	414	6516	5.1
TH1	34.3	356	4898	5.1
TH2	36	374	5539	5.0
LN	35.4	367	6098	4.7
LH1	45.5	472	6795	5.7
LH2	45	467	5440	6.3

At the end of each test, crack spacing over the constant moment region was measured. The final number of cracks, crack spacing, and average crack spacing for each specimen are as shown in Table 4.3-2. The cracks patterns with crack spacing dimensions are shown in Figure 4.3-5. Similar trends were observed when comparing the crack behavior from transverse specimens to the longitudinal specimens at same reinforcement arrangements. Comparing the ultimate load capacity to the resulting number of cracks, it is evident that as the specimen reached higher loads at failure, the number of cracks increased.

Table 4.3-2: Crack spacing in testing region at failure

Specimen ID	Flexural Reinforcement	Number of Cracks	Crack spacing (in.)	Average Crack Spacing (in.)
TN	Grade 60 at 9 in.	4	11-11-7-28	14.3
TH1	Grade 100 at 9 in.	7	9-7-6-12-8-10-11	9.0
TH2	Grade 100 at 15 in.	5	9-11-15-13-9	11.4
LN	Grade 60 at 9 in.	5	20-13-7-9-12	12.2
LH1	Grade 100 at 9 in.	7	17-5-7-8-7-8-11	9.0
LH2	Grade 100 at 15 in.	7	6-9-12-5-13-10	9.2

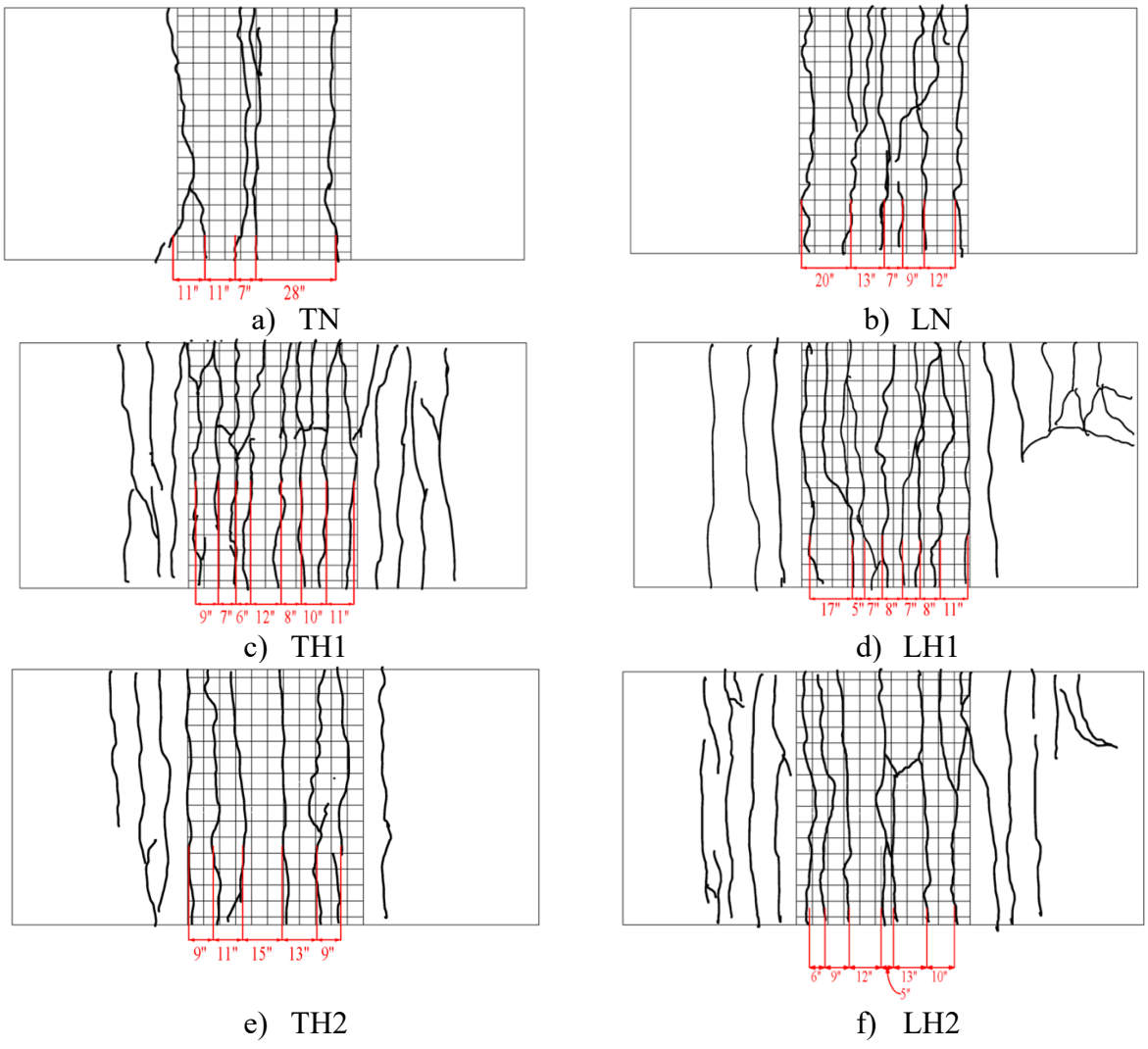

Figure 4.3-5: Crack patterns and crack spacing at failure

4.3.4. Transverse Specimens Crack-Control Results

The results for maximum crack width and average crack width for the transverse specimens are shown in Figure 4.3-6 and Figure 4.3-7. Although the number of cracks was greater for TH2 than TN, larger maximum and average crack widths were measured at similar load levels on TH2 than TN. Similarly, TH1 experienced smaller crack widths when compared to the control specimen.

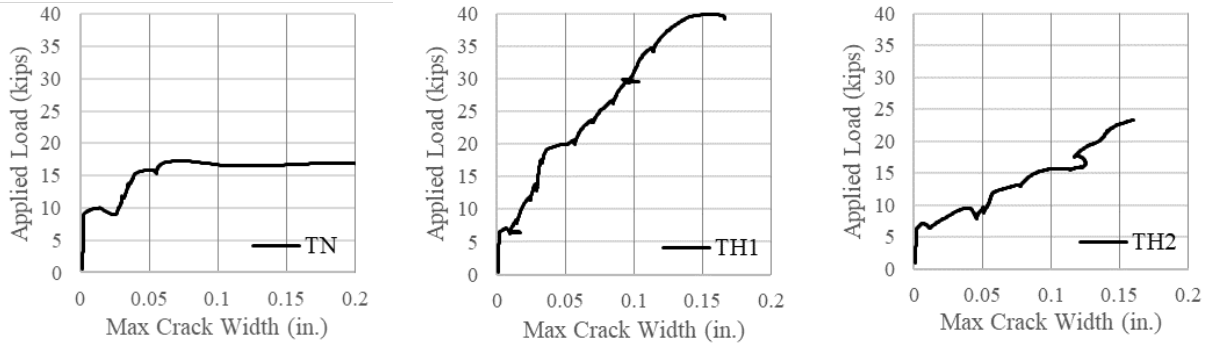

a) TN (Grade 60 @ 9 in.) b) TH1 (Grade 100 @ 9 in.) c) TH2 (Grade 100 @ 15 in.)

Figure 4.3-6: Maximum crack width results for transverse specimens

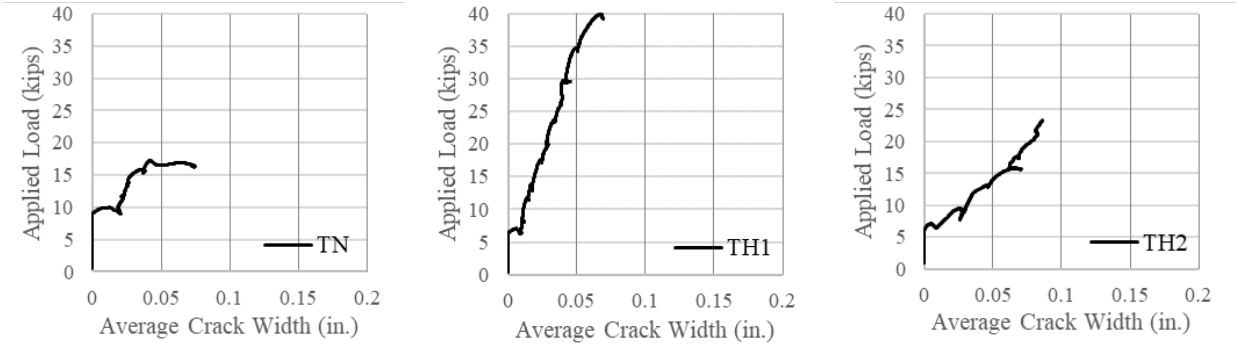

a) TN (Grade 60 @ 9 in.) b) TH1 (Grade 100 @ 9 in.) c) TH2 (Grade 100 @ 15 in.)

Figure 4.3-7: Average crack width results for transverse specimens

4.3.5. Longitudinal Specimens Crack-Control Results

The results for maximum crack width and average crack width for the longitudinal specimens are shown in Figure 4.3-8 and Figure 4.3-9. Similar results were observed in the transverse specimens on the longitudinal specimens. Generally, larger maximum and average crack widths were observed on TH2 at similar load levels when compared to LN.

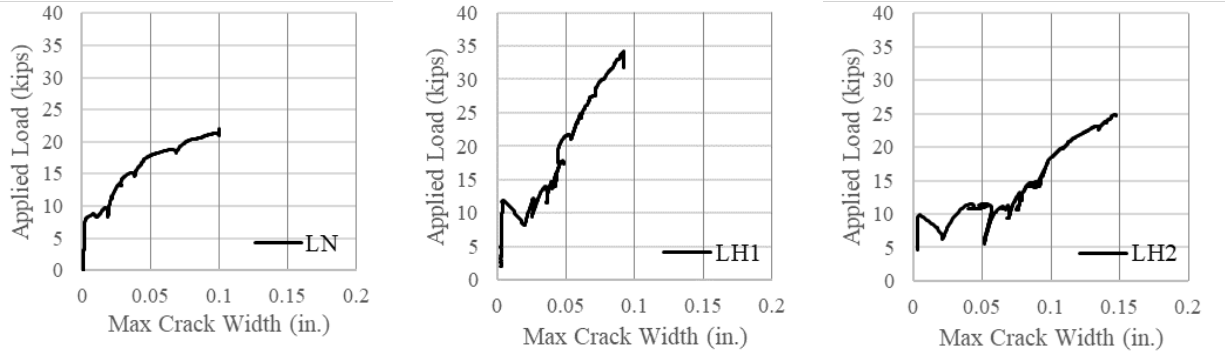

a) LN (Grade 60 @ 9 in.) b) LH1 (Grade 100 @ 9 in.) c) LH2 (Grade 100 @ 15 in.)

Figure 4.3-8: Maximum crack width results for longitudinal specimens

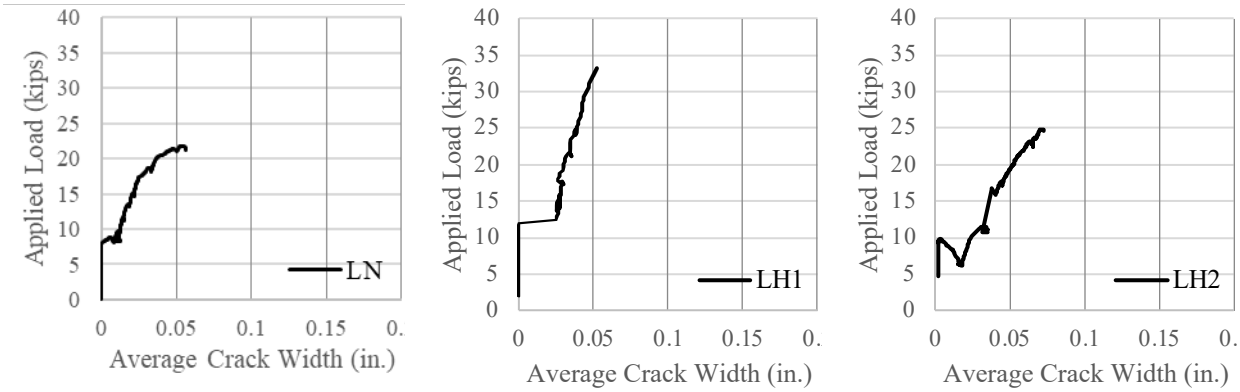

a) LN (Grade 60 @ 9 in.) b) LH1 (Grade 100 @ 9 in.) c) LH2 (Grade 100 @ 15 in.)

Figure 4.3-9: Average crack width results for longitudinal specimens

4.4. SEPARATION OF PANELS AT ULTIMATE LOADS

Current TxDOT standards specify an International Concrete Institute (ICRI) concrete surface preparation (CSP) No. 6 to No. 9 for surface roughening of PCPs surfaces. Assuming No.6 CSP has an approximate surface roughness amplitude of 1/8 in., this would be the smallest surface roughness amplitude allowed for PCP surfaces.

To be conservative, the surface roughness was assumed to be half of the smallest surface roughness amplitude, as shown in Figure 4.4-1. Therefore, complete separation of panels would be considered when the PI-gauges read the smallest surface roughness amplitude. When examining the results from the PI-gauges, excessive delamination was only detected in the LH1 and LH2 specimens at the ultimate stages of tests.

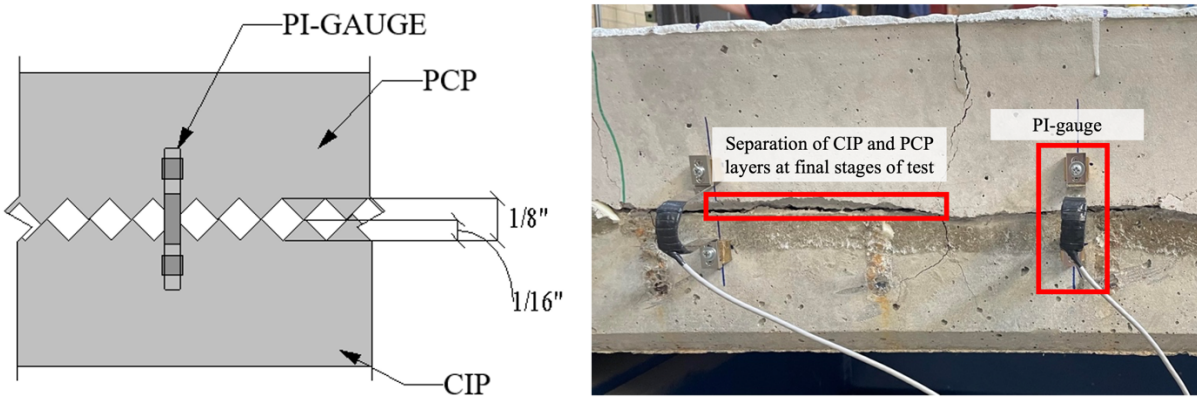

a) Separation of CIP and PCP layers

b) Separation of CIP and PCP layers at final stages of test

Figure 4.4-1: PI-gauge monitoring separation of CIP and PCP layers

Chapter 5: Evaluation of Experimental Results

In the previous chapter, the load-carrying and crack-control behavior for the longitudinal and transverse specimens were presented. In this chapter, the specimens will be compared to identify key aspects of behavior. For simplicity, only the average crack width will be used when comparing crack-control behavior.

5.1. Comparisons of Load Capacity

To examine the implementation of high-strength reinforcement in the CIP portion of the deck strip specimens, each arrangement was compared to the control specimen in the respective direction. To easily compare the effects of increased rebar grade, the transverse specimen TH1 and longitudinal specimen LH1 was plotted with their respective control specimen, as shown in Figure 5.1-1. It is observed that when increasing the reinforcement grade from 60 ksi to 100 ksi at the same spacing, specimens with increased rebar grade exhibited larger ultimate applied load and deflections.

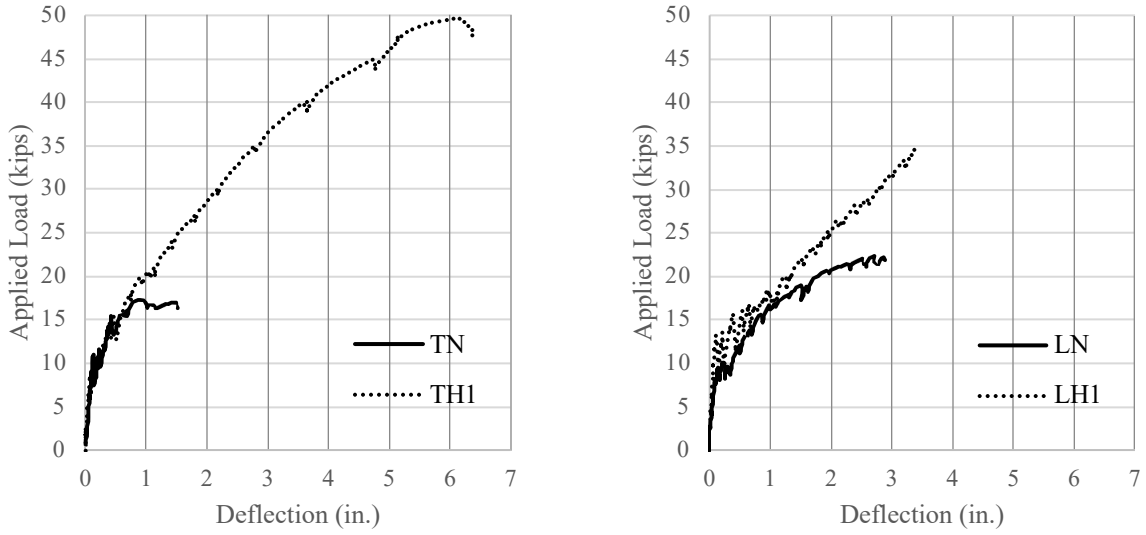

a) Transverse Specimens b) Longitudinal Specimens

Figure 5.1-1: Load-Deflection for rebar grade

To compare the effects of increased rebar grade at a larger spacing, the transverse specimen TH2 and longitudinal specimen LH2 were plotted with their respective control specimen, as shown in Figure 5.1-2. When analyzing the specimens with increased rebar grade at larger spacing, the longitudinal and transverse specimens had similar initial stiffness as the control specimen. Regarding ultimate capacity, it is evident that the specimens equipped with grade 100 reinforcement at 15 in. were able to carry a larger load than the control specimen in both loading directions.

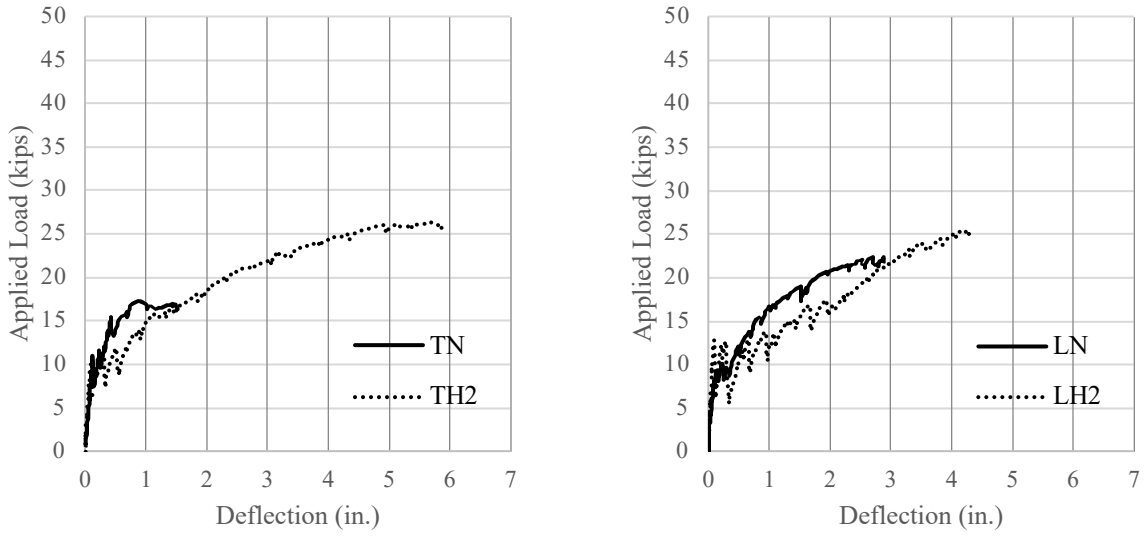

a) Transverse Specimens b) Longitudinal Specimens

Figure 5.1-2: Load-Deflection for rebar arrangement

Overall, there seems to be a similar trend when comparing the change of rebar arrangement for the transverse and longitudinal specimens regarding load capacity. As shown in Figure 5.1-3, increasing the grade of reinforcement while keeping the same amount of reinforcement in the CIP layer results in an increase in load capacity. When the grade of reinforcement is increased and the amount is decreased, the load capacity is slightly larger than the specimen equipped with conventional reinforcement in the CIP layer. Therefore, the specimens with high-strength

reinforcement in the CIP layer performed satisfactorily in terms of load capacity when compared to the control specimens.

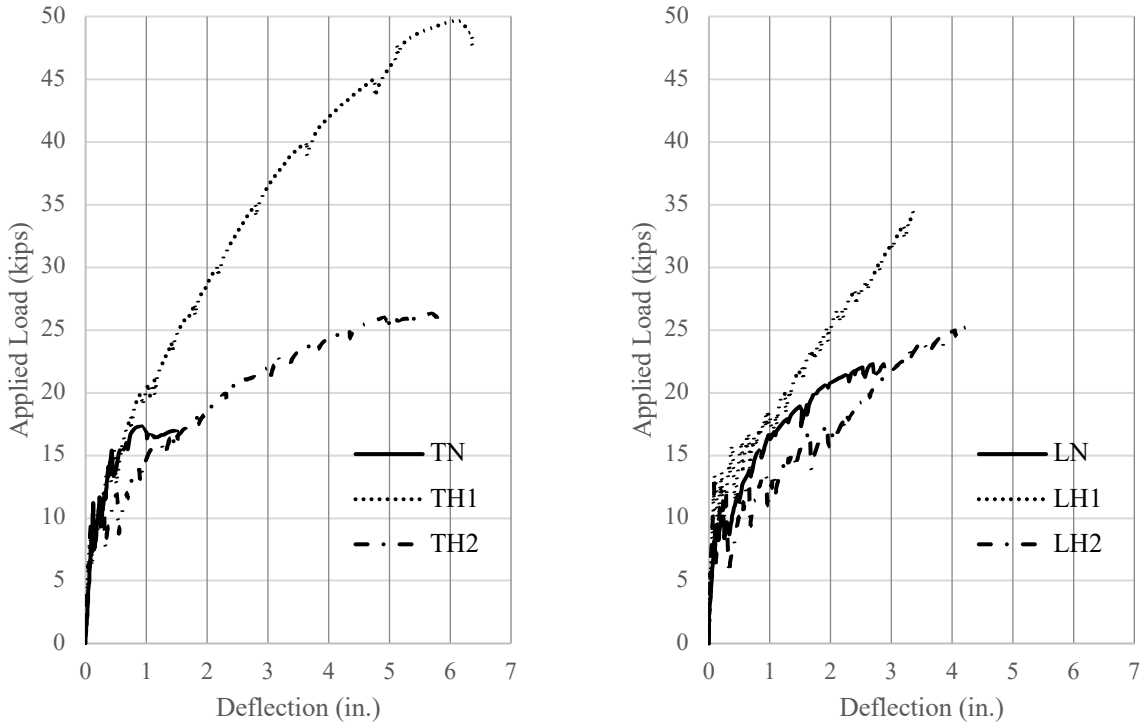

a) Transverse Specimens b) Longitudinal Specimens

Figure 5.1-3: Load-Deflection for all rebar specimens

5.2. COMPARISONS OF CRACK-CONTROL PERFORMANCE

This section presents a comparison in crack-control performance by comparing the crack behavior in terms of loading directions and reinforcement arrangement.

To identify the crack-control performance of specimens with high-strength reinforcement, specimens were compared to the control specimen by average crack widths. As shown in Figure 5.2-1, the specimens with high-strength reinforcement at 9 in. were compared to the respective control specimen. Although the initial crack width differed from each specimen, generally similar crack widths were apparent in lower load levels. The transverse specimens had similar crack

widths up to the applied load of 15 kips and the longitudinal specimens had similar crack widths up to 17.5 kips. After these load levels, the crack widths began to differ due to yielding of the TN and LN specimens. These comparisons show that increasing the grade while keeping the same reinforcement spacing produces similar crack-control performance as the control specimens at lower load levels.

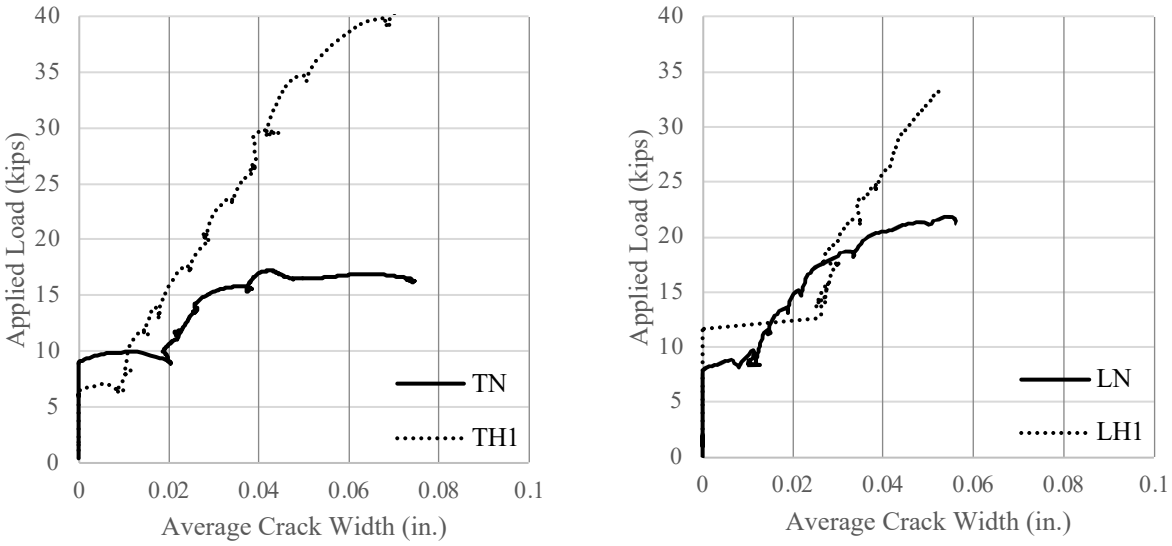

a) Transverse Specimens b) Longitudinal Specimens

Figure 5.2-1: Crack-control behavior for rebar grade

When analyzing the use of high-strength reinforcement at a greater spacing, specimens TH2 and LH2 were compared to the control specimens. For the majority of the loading duration, specimens TH2 and LH2 had larger crack widths compared to TN and LN, as shown in Figure 5.2-2. As the control specimens reached failure, specimens TH2 and LH2 approached similar crack widths as TN and LN. Based on the larger crack widths at lower loads, high-strength reinforcement at larger spacing is shown to negatively impact crack-control performance.

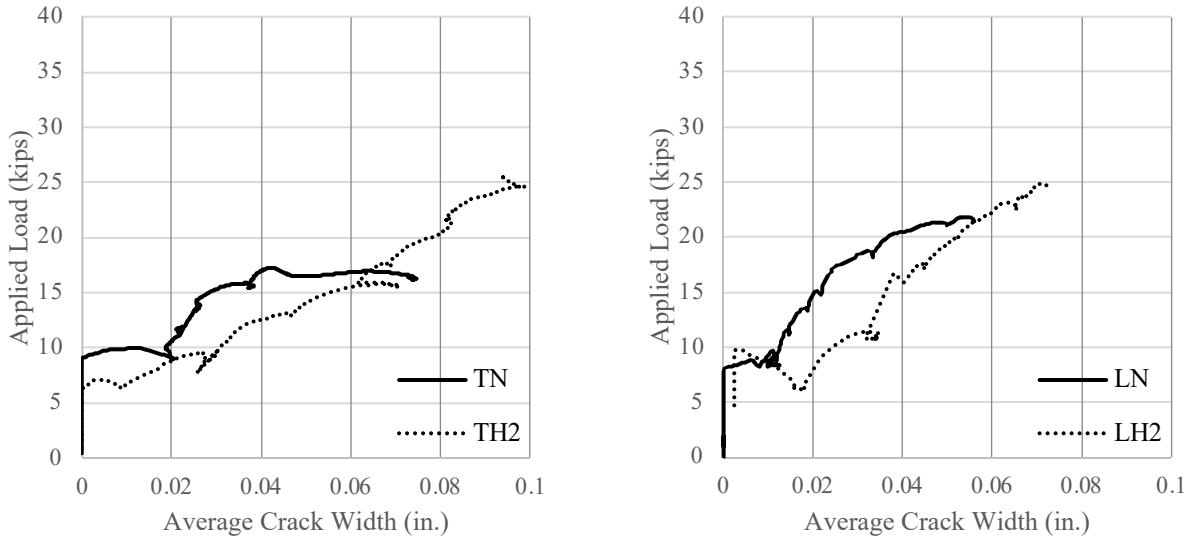

a) Transverse Specimens b) Longitudinal Specimens

Figure 5.2-2: Crack-control behavior with optimized reinforcement arrangement

Ultimately, these results show that the only high-strength reinforcement alternative that has similar crack-control as the control specimens is #4 at 9 in. All average crack width results are compiled per specimen series in Figure 5.2-3.

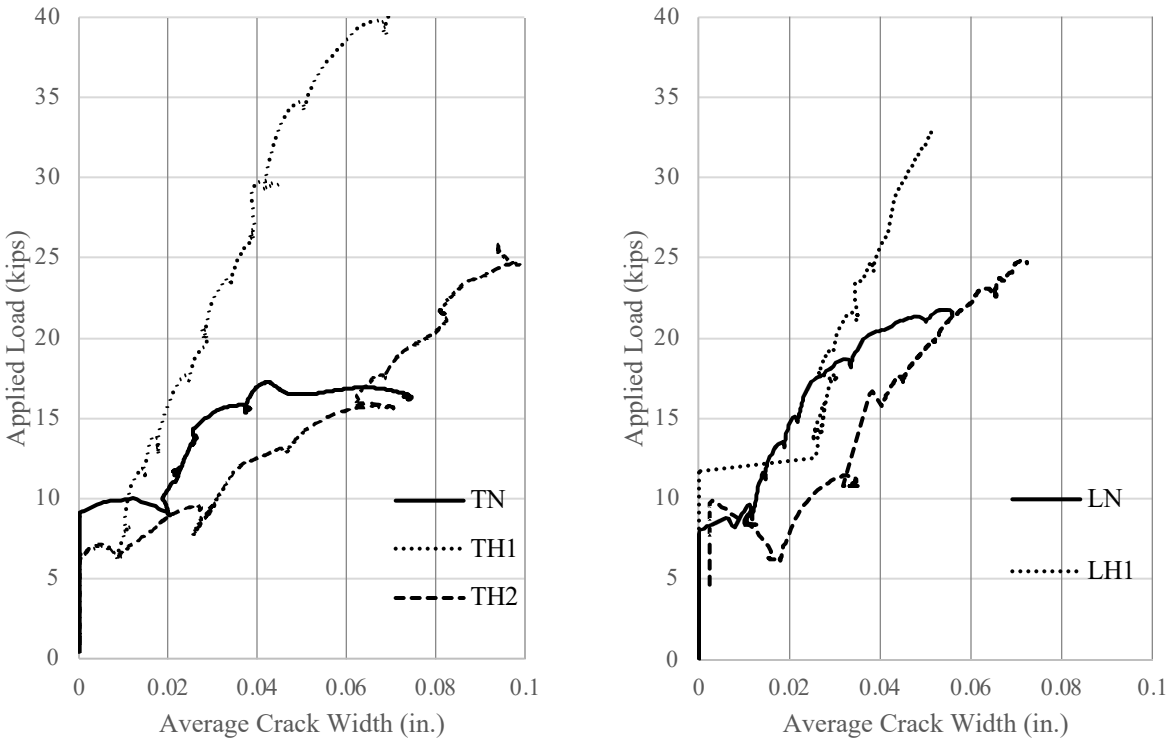

a) Transverse Specimens b) Longitudinal Specimens

Figure 5.2-3: Crack-control behavior for all rebar arrangements

5.3. TEST LOADING AND FIELD LOADING COMPARISONS

When comparing the flexural deck strip tests to the loading conditions in the field, differences in cracking behavior should be noted. Most cracks in CIP-PCP bridge decks occur due to restrained shrinkage effect of PCPs on the CIP layer (Folliard, 2003). The difference in cracking behavior from the flexural tests conducted in this study and that in field loading conditions result in a difference of concrete tensile stress prior to cracking. Assuming the same concrete strength and concrete tensile forces in flexure and axial to be the calculated modulus of rupture ($7.5\sqrt{f'_c}$) and direct tension ($4\sqrt{f'_c}$) stresses, the estimated reinforcement stress at cracking are shown in Figure 5.3-1. It is observed that reinforcement in field loading conditions experiences an increase of 12% in rebar stress when compared to the deck strip flexural tests. Therefore, a constraint

associated with utilizing deck strip flexural tests is that their inability to precisely replicate the boundary conditions experienced in field loading.

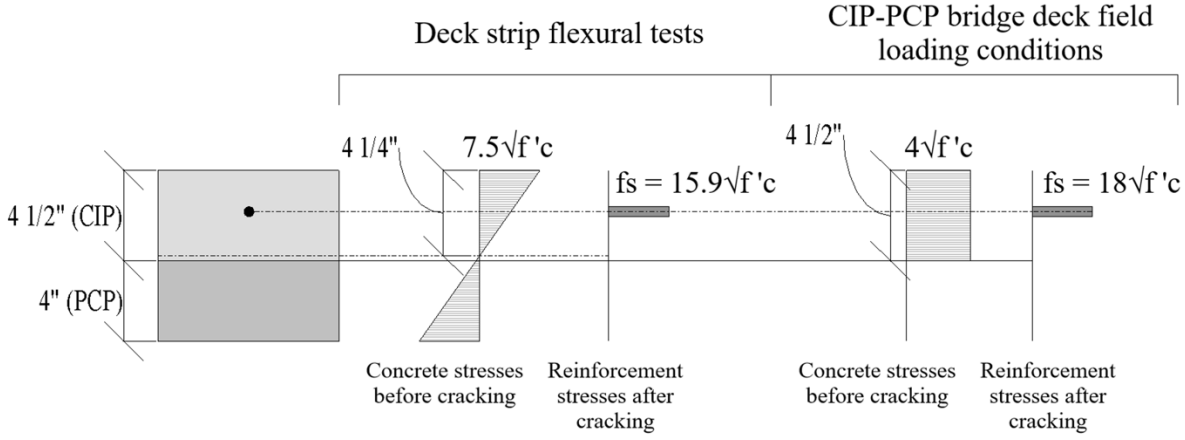

Figure 5.3-1: Comparison of test and field loading conditions

Chapter 6: Summary and Conclusions

This chapter explains the objective of the study, conclusions made from experimental results, and recommendations for future work.

6.1. SUMMARY OF WORK

The focus of the study was to examine the use of high-strength reinforcement in CIP-PCP bridge decks. Deck strip specimens, which simulate transverse and longitudinal panel joint and reinforcement details in CIP-PCP bridge decks, were tested in four-point bending. A total of six deck strip specimens were fabricated, with three simulating the transverse section details and three simulating the longitudinal section details. Each set of specimens consisted of three reinforcement arrangements to highlight the influence of high-strength reinforcement as the longitudinal and transverse reinforcement in CIP-PCP bridge decks. These specimens were evaluated by the load capacity and crack-control performance. From the experimental tests and comparisons, the following conclusions can be drawn:

1. The use of high-strength reinforcement at 9 in. resulted in greater flexural capacity and similar crack widths at lower stages of loading when compared to conventional reinforcement at 9 in.
2. The use of high-strength reinforcement at 15 in. resulted in slightly larger flexural capacity and larger crack widths at lower stages of loading when compared to conventional reinforcement at 9 in.

6.2. RECOMMENDATIONS

The following recommendations are made based on the deck strip test results conducted in this experimental program:

1. The only high-strength reinforcement arrangement that should be considered in CIP-PCP bridge decks is #4 Grade 100 at 9 in.
2. To validate the findings of this report, an implementation study should be conducted to further analyze the use of high-strength reinforcement in CIP-PCP bridge deck field conditions.

Appendix A: Stress-Strain Curves of Steel Reinforcement Material Tests

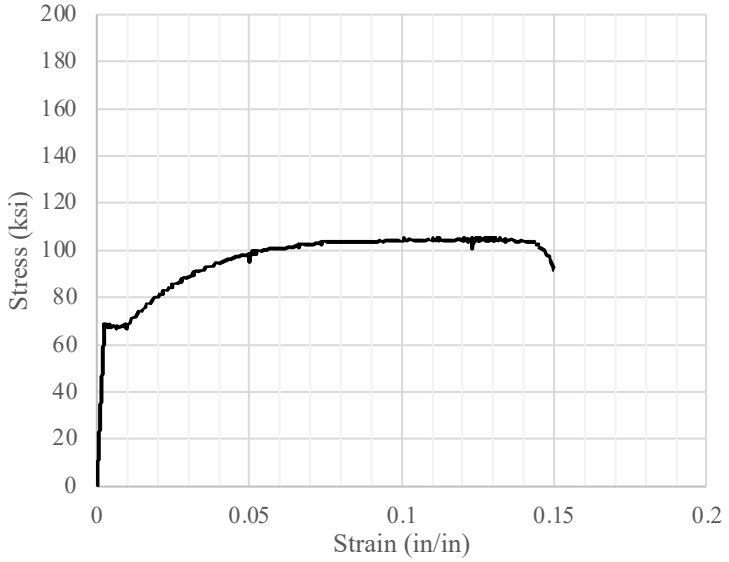

Figure A-1: Stress-strain curve for ASTM A615 #4 (Specimen TN)

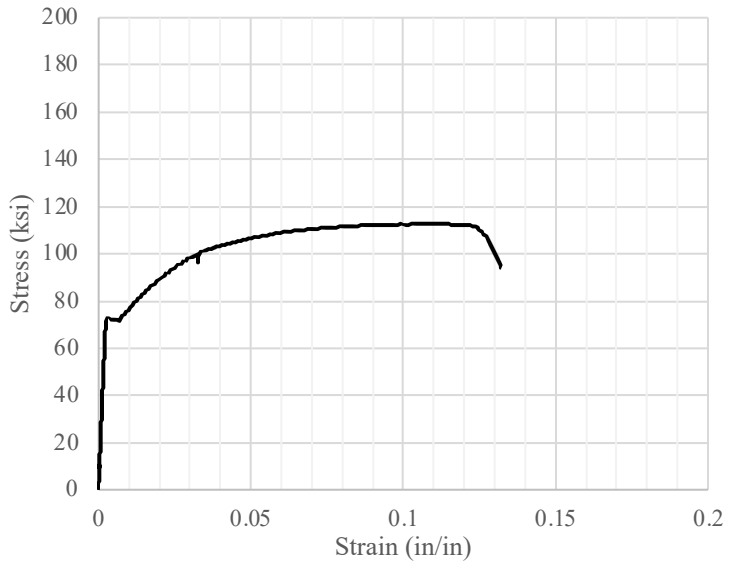

Figure A-2: Stress-strain curve for ASTM A615 #4 (Specimen LN)

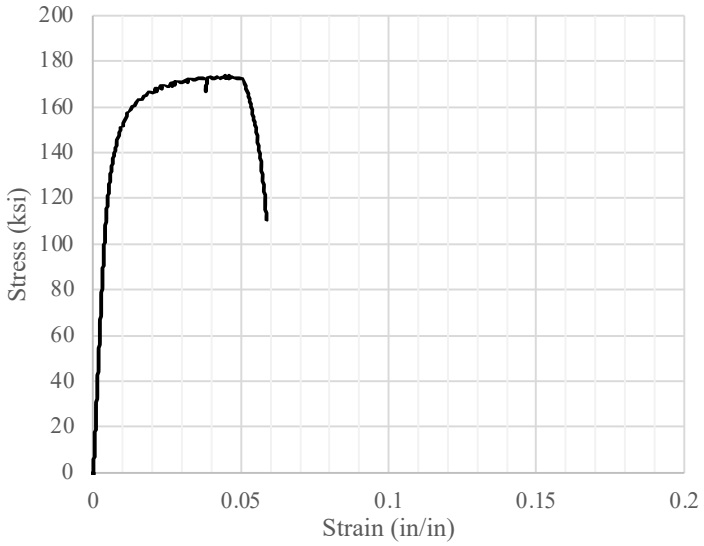

Figure A-3: Stress-strain curve for ASTM A1035 #4

References

ACI 318-19 Building Code Requirements for Structural Concrete and Commentary. (2019). American Concrete Institute. https://doi.org/10.14359/51716937

Aldabagh, S., & Alam, M. S. (2020). High-Strength Steel Reinforcement (ASTM A1035/A1035M Grade 690): State-of-the-Art Review. *Journal of Structural Engineering*, *146*(8), 03120003. https://doi.org/10.1061/(ASCE)ST.1943-541X.0002720

ASTM A370: Test Methods and Definitions for Mechanical Testing of Steel Products. (2023). ASTM International. https://doi.org/10.1520/A0370-23

ASTM C39/C39M: Test Method for Compressive Strength of Cylindrical Concrete Specimens. (2021). ASTM International. https://doi.org/10.1520/C0039_C0039M-21

ASTM C143/C143M: Standard Test Method for Slump of Hydraulic-Cement Concrete. (2020). ASTM International. https://doi.org/10.1520/C0143_C0143M

ASTM C469/C469M: Test Method for Static Modulus of Elasticity and Poissons Ratio of Concrete in Compression. (2022). ASTM International. https://doi.org/10.1520/C0469_C0469M-22

ASTM C496/C496M: Test Method for Splitting Tensile Strength of Cylindrical Concrete Specimens. (2017). ASTM International. https://doi.org/10.1520/C0496_C0496M-17

Buth, E., Furr, H. L., & Jones, H. L. (1972). *Evaluation of a Prestressed Panel, Cast-In-Place Concrete Bridge*.

Folliard, K. (2003). *Evaluation of Alternative Materials to Control Drying-Shrinkage Cracking in Concrete Bridge Decks*.

Foster, S. (2010). *Reducing Top Mat Reinforcement in Bridge Decks*.

Frosch, R. (1999). Another Look at Cracking and Crack Control in Reinforced Concrete. *ACI Structural Journal*, *96*(3). https://doi.org/10.14359/679

Frosch, R., Labi, S., & Sim, C. (2014). *Increasing Bridge Deck Service Life: Volume I—Technical Evaluation*. Purdue University. https://doi.org/10.5703/1288284315516

Kahl, S. (2007). *CORROSION RESISTANT ALLOY STEEL (MMFX) REINFORCING BAR IN BRIDGE DECKS* (R-1499). Michigan Department of Transportation.

Kareem, R. (2020). *Behavior of Concrete Structures Reinforced with High Strength Steel*.

Kareem, R. S., Jones, C., Dang, C. N., Prinz, G. S., & Micah Hale, W. (2020). Structural performance of concrete bridge decks reinforced with Grade-830 steel bars. *Structures*, *27*, 1396–1404. https://doi.org/10.1016/j.istruc.2020.07.054

Kwon, K. Y. (2012). *Design Recommendations for CIP-PCP Bridge Decks*.

Merrill, B. D. (2002). *TEXAS' USE OF PRECAST CONCRETE STAY-IN-PLACE FORMS FOR BRIDGE DECKS.*

Prestressed Concrete Panel Fabrication Details. (2023). https://ftp.txdot.gov/pub/txdot-info/Pre-Letting%20Responses/Waco%20District/Construction%20Projects/Archive/FY%202020/018-April%202020/0808-01-061,%20FM%20413,%20Falls%20Co./PCP-FAB.PDF